

# Deep Fréchet Regression

Su I Iao\*, Yidong Zhou\*, Hans-Georg Müller  
Department of Statistics, University of California, Davis

June 11, 2024

## Abstract

Advancements in modern science have led to the increasing availability of non-Euclidean data in metric spaces. This paper addresses the challenge of modeling relationships between non-Euclidean responses and multivariate Euclidean predictors. We propose a flexible regression model capable of handling high-dimensional predictors without imposing parametric assumptions. Two primary challenges are addressed: the curse of dimensionality in nonparametric regression and the absence of linear structure in general metric spaces. The former is tackled using deep neural networks, while for the latter we demonstrate the feasibility of mapping the metric space where responses reside to a low-dimensional Euclidean space using manifold learning. We introduce a reverse mapping approach, employing local Fréchet regression, to map the low-dimensional manifold representations back to objects in the original metric space. We develop a theoretical framework, investigating the convergence rate of deep neural networks under dependent sub-Gaussian noise with bias. The convergence rate of the proposed regression model is then obtained by expanding the scope of local Fréchet regression to accommodate multivariate predictors in the presence of errors in predictors. Simulations and case studies show that the proposed model outperforms existing methods for non-Euclidean responses, focusing on the special cases of probability measures and networks.

*Keywords:* curse of dimensionality, deep learning, Fréchet regression, non-Euclidean data, Wasserstein space.

---

\*These authors contributed equally to this work

# 1 Introduction

Regression analysis serves as the cornerstone of statistical methodology, providing a fundamental framework for modeling complex relationships between response and predictor variables. The demand for comprehensive and versatile regression techniques has soared, driven by the prevalence of non-Euclidean responses. These responses encompass a broad spectrum of data types, ranging from networks (Zhou and Müller, 2022), covariance matrices (Dryden et al., 2009) and trees (Nye et al., 2017) to distributions (Petersen et al., 2022) and other complex structures.

Real-world applications across various domains underscore the need for advanced regression methods. For instance, in transportation science, understanding the evolution of transportation networks in response to factors like weather conditions and public health data is of paramount interest (Tucker et al., 2023). These and related scenarios are covered by a general approach where one views the responses as random objects situated in metric spaces (Müller, 2016). Challenges that we address in this paper include the absence of linear structure and the potential high dimensionality of multivariate predictors.

Regression with metric-space valued responses is thus of paramount interest. Early explorations include regression for non-Euclidean data using Euclidean embedding with distance matrices (Faraway, 2014) and a Nadaraya-Watson kernel regression approach (Hein, 2009). A Fréchet regression approach was introduced more recently (Petersen and Müller, 2019; Chen and Müller, 2022; Schötz, 2022). It extends linear and nonparametric regression techniques to accommodate metric-space valued responses through conditional Fréchet means. However, these regression models either rely on strict assumptions akin to classical linear models for scalar responses or suffer from the curse of dimensionality in analogy to traditional nonparametric regression.

In practical applications, the need often arises to flexibly model metric-space valued responses with potentially high-dimensional predictors, so that these limitations prevent application of these methods for real-world challenges. Several recent works considered extending sufficient dimension reduction approaches (Ying and Yu, 2022; Zhang et al., 2023), single index models (Bhattacharjee and Müller, 2023), and principal component regression (Song and Han, 2023) to Fréchet regression to address high-dimensionality of the predictors. These methods, while capable of reducing predictor dimensionality, are confined to the construction of a universal kernel or strong assumptions similar to those for classical single index and linear models.

To address these limitations, we harness deep learning (LeCun et al., 2015), taking advantage of its capability of handling high-dimensional predictors without compromising model flexibility. Deep learning is known for its capacity to automatically extract features from complex data, but has not been developed so far for non-Euclidean responses. The proposed regression model utilizes manifold learning (Ghojogh et al., 2023) for the observed metric-space valued responses, generating low-dimensional representations. Manifold learning is a nonlinear dimensionality reduction technique that has proven useful for dimensionality reduction of infinite-dimensional functional data (Chen and Müller, 2012), where data are assumed to lie on a low-dimensional manifold that is unknown. Indeed, many data residing in metric spaces, including parametric families of probability distributions or stochastic block models for networks, are expected to have such a low-dimensional manifold structure; we exploit such structure for the proposed statistical modeling.

We deploy a deep neural network that takes the observed predictors as input and produces the low-dimensional manifold representation as output. One key innovation of the proposed approach is that we demonstrate that local Fréchet regression can be utilized

to map the low-dimensional manifold representation to the original metric space so that the final output resides in the metric space where the random objects are situated. This map, which has not yet been considered in the manifold learning literature for metric-space valued data, is crucial for the implementation of a regression model in statistics, as it is mandatory for interpretability to predict the random objects residing in metric spaces, rather than their low-dimensional representations. This comprehensive framework makes it possible to handle high-dimensional predictors while concurrently accommodating the complexities intrinsic to metric-space valued responses.

Our key contributions are as follows. First, we utilize deep learning for Fréchet regression, highlighting its efficacy as a powerful tool for the regression of metric-space valued responses. Second, our model can handle high-dimensional predictors for metric-space valued data that allow a manifold representation. Third, we investigate the convergence rate of deep neural networks in the presence of dependent sub-Gaussian noise accompanied by bias. This analysis is conducted under a well-established general composition assumption on the regression function ([Schmidt-Hieber, 2020](#)), which necessitates an extension of the existing theoretical framework due to the presence of dependence and bias. Although [Bos and Schmidt-Hieber \(2023\)](#) introduced the convergence rate of deep neural networks with dependent and non-central response variables, their findings are limited to local dependence, while the dependence considered here does not rely on any specific form and is not restricted to local dependence. Fourth, we demonstrate how local Fréchet regression can be used to map the low-dimensional representation back to the original metric space, for which we establish convergence in the presence of errors in predictors. Fifth, we examine the asymptotic properties of the proposed regression model, including its rate of convergence. Lastly, we showcase results from various simulation settings and two real-data applica-

tions, demonstrating the superior performance of the proposed regression model compared to existing approaches.

The structure of the paper is as follows. In Section 2, we introduce notation and provide background on deep neural networks and local Fréchet regression. The proposed regression model is introduced in Section 3, with the asymptotic convergence rate established in Section 4. Simulation results for distributional data are presented in Section 5. The proposed framework is illustrated in Section 6 using networks arising from the New York yellow taxi records. Finally, we conclude with a brief discussion in Section 7. Auxiliary results and proofs as well as additional simulations for networks and a second data application for age-at-death distributions of human mortality are provided in the Supplementary Material.

## 2 Preliminaries

### 2.1 Notation

Let  $\mathbb{R}$  represent the set of real numbers and  $\mathbb{R}_+$  denote the set of all positive real numbers. The set of all positive natural numbers is denoted as  $\mathbb{N}_+$ . Throughout this work, plain letters refer to (random) scalars and bold letters refer to (random) vectors. For a vector  $\mathbf{v}$ , we define  $\mathbf{v}^{\oplus 0} = 1, \mathbf{v}^{\oplus 1} = \mathbf{v}, \mathbf{v}^{\oplus 2} = \mathbf{v}\mathbf{v}^T$ . We let  $\|\cdot\|$  denote a norm and set  $\|\cdot\| = \|\cdot\|_2$  (the Euclidean norm for vectors) by default unless stated otherwise. Additionally,  $\|\cdot\|_0$  denotes the number of nonzero entries of a matrix or vector, and  $\|\cdot\|_\infty$  represents the sup-norm for vectors, matrices, or functions. The notation  $a \lesssim b$  implies the existence of a positive constant  $C$  such that  $a \leq Cb$ . Moreover,  $a \asymp b$  if both  $a \lesssim b$  and  $b \lesssim a$ . Finally,  $a \wedge b = \min\{a, b\}, a \vee b = \max\{a, b\}$ .

## 2.2 Deep neural networks

We provide an overview of deep neural networks (DNNs) as function approximations. The focus lies on the nonparametric regression model with  $p$ -dimensional covariates in the unit hypercube, represented by observations  $(\mathbf{X}_i, U_i) \in [0, 1]^p \times \mathbb{R}$ . Consider the following regression model

$$U_i = g_0(\mathbf{X}_i) + \epsilon_i, \quad i = 1, \dots, n, \quad (1)$$

where  $g_0$  is an unknown function and  $\epsilon_i$  is independent and identically distributed (i.i.d.) noise with zero mean and finite variance.

A DNN with  $L$  hidden layers and layer width  $\mathbf{p} = (p_0, \dots, p_L, p_{L+1})^\top$  is defined recursively, forming a composite function  $g : \mathbb{R}^{p_0} \mapsto \mathbb{R}^{p_{L+1}}$ ,

$$\begin{aligned} g(\mathbf{x}) &= W_L g_L(\mathbf{x}) + \mathbf{b}_L, \\ g_L(\mathbf{x}) &= \sigma\{W_{L-1} g_{L-1}(\mathbf{x}) + \mathbf{b}_{L-1}\}, \dots, g_1(\mathbf{x}) = \sigma(W_0 \mathbf{x} + \mathbf{b}_0), \end{aligned} \quad (2)$$

where  $W_l \in \mathbb{R}^{p_{l+1} \times p_l}$  is a weight matrix and  $\mathbf{b}_l \in \mathbb{R}^{p_{l+1}}$  is a shift vector for  $l = 0, \dots, L$ . The rectifier linear unit (ReLU) activation function  $\sigma = \max\{0, x\}$  (Nair and Hinton, 2010) operates component-wise, that is,  $\sigma\{(x_1, \dots, x_{p_l})^\top\} = (\sigma(x_1), \dots, \sigma(x_{p_l}))^\top$ . We focus on the ReLU activation function for its widespread use, empirical success, and theoretical support (LeCun et al., 2015). Observe that  $p_0 = p$  and  $p_{L+1} = 1$  in the case of nonparametric regression with  $p$ -dimensional covariates.

Given  $L \in \mathbb{N}_+$ ,  $\mathbf{p} \in \mathbb{N}_+^{L+2}$ ,  $s \in \mathbb{N}_+$  and a constant  $D > 0$ , in analogy to Schmidt-Hieber (2020), we consider a class of sparse neural networks

$$\begin{aligned} \mathcal{G}(L, s, \mathbf{p}, D) &= \{g \text{ of the form (2): } \max_{l=0, \dots, L} \{\|W_l\|_\infty, \|\mathbf{b}_l\|_\infty\} \leq 1, \\ &\quad \sum_{l=1}^L \|W_l\|_0 + \|\mathbf{b}_l\|_0 \leq s, \|g\|_\infty \leq D\}. \end{aligned} \quad (3)$$

We focus on DNNs with bounded weight matrices and shift vectors. This choice is motivated by empirical observations where the learned matrices and vectors tend to remain relatively small, especially when initialized with modest-sized matrices and vectors. Additionally, the consideration of sparse neural networks arises from the practical issue of overfitting deep feedforward neural networks with fully connected layers. This concern is addressed by pruning weights, reducing the total number of nonzero parameters, and sparsely connecting layers (Han et al., 2015; Srinivas et al., 2017).

To estimate the regression function  $g_0$ , the basic paradigm is to minimize the empirical risk

$$\hat{g} = \arg \min_{g \in \mathcal{G}} \frac{1}{n} \sum_{i=1}^n \{U_i - g(\mathbf{X}_i)\}^2.$$

Certain restrictions on the regression function  $g_0$  are necessary to study the asymptotic properties of the estimator  $\hat{g}$ . Consider the Hölder class of smooth functions, where the ball of  $\beta$ -Hölder functions with radius  $M > 0$  is

$$\mathcal{H}_p^\beta(\mathbb{D}, M) = \{g : \mathbb{D} \subset \mathbb{R}^p \mapsto \mathbb{R} : \sum_{\alpha: |\alpha| < \beta} \|\partial^\alpha g\|_\infty + \sum_{\alpha: |\alpha| = \lfloor \beta \rfloor} \sup_{\mathbf{x}, \mathbf{y} \in \mathbb{D}, \mathbf{x} \neq \mathbf{y}} \frac{|\partial^\alpha g(\mathbf{x}) - \partial^\alpha g(\mathbf{y})|}{\|\mathbf{x} - \mathbf{y}\|_\infty^{\beta - \lfloor \beta \rfloor}} \leq M\},$$

where  $\lfloor \beta \rfloor$  denotes the largest integer strictly smaller than  $\beta$ ,  $\partial^\alpha = \partial^{\alpha_1} \dots \partial^{\alpha_p}$  with  $\alpha = (\alpha_1, \dots, \alpha_p)^\top$ , and  $|\alpha| = \sum_{k=1}^p \alpha_k$ . Let  $q \in \mathbb{N}$ ,  $\beta = (\beta_0, \dots, \beta_q)^\top \in \mathbb{R}_+^{q+1}$  and  $\mathbf{d} = (d_0, \dots, d_{q+1})^\top \in \mathbb{N}_+^{q+2}$ ,  $\tilde{\mathbf{d}} = (\tilde{d}_0, \dots, \tilde{d}_q)^\top \in \mathbb{N}_+^{q+1}$  with  $\tilde{d}_j \leq d_j, j = 0, \dots, q$ . We assume that the regression function  $g_0$  belongs to a composite smoothness function class:

$$\begin{aligned} \mathcal{H}(q, \beta, \mathbf{d}, \tilde{\mathbf{d}}, M) = & \{g = g_q \circ \dots \circ g_0 : g_j = (g_{j1}, \dots, g_{jd_{j+1}})^\top \text{ and} \\ & g_{jk} \in \mathcal{H}_{\tilde{d}_j}^{\beta_j}([a_j, b_j]^{\tilde{d}_j}, M), \text{ for some } |a_j|, |b_j| \leq M\}. \end{aligned} \quad (4)$$

Functions in this class are characterized by two kinds of dimensions,  $\mathbf{d}$  and  $\tilde{\mathbf{d}}$ , where the

latter represents the intrinsic dimension of the function. For example, if

$$g(\mathbf{x}) = g_{31}(g_{21}[g_{11}\{g_{01}(x_1) + g_{02}(x_2)\} + g_{12}\{g_{03}(x_3) + g_{04}(x_4)\}] \\ + g_{22}[g_{13}\{g_{05}(x_5) + g_{06}(x_6)\} + g_{14}\{g_{07}(x_7) + g_{08}(x_8)\}]), \quad \mathbf{x} \in [0, 1]^8 \quad (5)$$

and  $g_{ij}$  are twice continuously differentiable, then smoothness  $\boldsymbol{\beta} = (2, 2, 2, 2)^\top$ , dimensions  $\mathbf{d} = (8, 8, 4, 2, 1)^\top$  and  $\tilde{\mathbf{d}} = (1, 1, 1, 1)^\top$ . The composite smoothness class  $\mathcal{H}(q, \boldsymbol{\beta}, \mathbf{d}, \tilde{\mathbf{d}}, M)$  contains a rich set of classical smoothness classes and has been widely adopted (Bauer and Kohler, 2019; Schmidt-Hieber, 2020; Kohler and Langer, 2021).

Writing

$$\kappa_n = \max_{j=0, \dots, q} n^{-\tilde{\beta}_j / (2\tilde{\beta}_j + \tilde{d}_j)} \text{ with } \tilde{\beta}_j = \beta_j \prod_{k=j+1}^q (\beta_k \wedge 1), \quad (6)$$

we require the following common assumption on the structure of the DNN model (Schmidt-Hieber, 2020; Zhong et al., 2022).

$$(D1) \quad D \geq \max\{M, 1\}, \quad L = O(\log n), \quad s = O(n\kappa_n^2 \log n) \text{ and } n\kappa_n^2 \lesssim \min_{l=1, \dots, L} p_l \leq \\ \max_{l=1, \dots, L} p_l \lesssim n.$$

Assumption (D1) characterizes the flexibility of the neural network family  $\mathcal{G}(L, s, \mathbf{p}, D)$  as per (3). While more flexible neural networks (with increased depth and width) are capable of achieving smaller approximation errors (Anthony et al., 1999; Schmidt-Hieber, 2020), they often introduce larger estimation errors. Thus, Assumption (D1) provides a balance between approximation and estimation errors.

### 2.3 Local Fréchet regression

Let  $(\Omega, d)$  be a totally bounded metric space with distance  $d : \Omega \times \Omega \mapsto [0, \infty)$  and  $\mathcal{T}$  be a closed interval in  $\mathbb{R}$ . Consider a random pair  $(\mathbf{Z}^0, Y)$  with a joint distribution  $F$  supported on the product space  $\mathcal{T}^r \times \Omega$ . We denote the marginal distributions of  $\mathbf{Z}^0$  and  $Y$



as  $F_{\mathbf{Z}^0}$  and  $F_Y$ , respectively, and the conditional distribution of  $Y$  given  $\mathbf{Z}^0$  as  $F_{Y|\mathbf{Z}^0}$ . The Fréchet mean and Fréchet variance of random objects in metric spaces (Fréchet, 1948), as generalizations of usual notions of mean and variance, are defined as

$$y_{\oplus} = \arg \min_{y \in \Omega} E\{d^2(Y, y)\}, \quad V_{\oplus} = E\{d^2(Y, y_{\oplus})\},$$

where the existence and uniqueness of the minimizer depend on the structural properties of the underlying metric space and are guaranteed for Hadamard spaces.

The conditional Fréchet mean of  $Y$  given  $\mathbf{Z}^0 = \mathbf{z}$ , corresponding to the regression function, is

$$v(\mathbf{z}) = \arg \min_{y \in \Omega} Q(y, \mathbf{z}), \quad Q(\cdot, \mathbf{z}) = E\{d^2(Y, \cdot) | \mathbf{Z}^0 = \mathbf{z}\}. \quad (7)$$

The lack of an algebraic structure in general metric spaces poses challenges in modeling and estimating the regression function  $v(\mathbf{z})$ . To address this challenge, previous work (Petersen and Müller, 2019) suggested leveraging the algebraic structure within the predictor space  $\mathcal{T}^r$ . Let  $K$  be an  $r$ -dimensional kernel corresponding to a symmetric  $r$ -dimensional probability density function and write  $K_h(\mathbf{z}) = h^{-r} K(H^{-1}\mathbf{z})$  with  $H = hI_r$  for a suitably chosen bandwidth  $h$ . Extending local linear regression to metric-space valued responses (Petersen and Müller, 2019), local Fréchet regression (LFR) models conditional Fréchet mean  $v(\mathbf{z})$  as a weighted Fréchet mean,

$$v_h(\mathbf{z}) = \arg \min_{y \in \Omega} Q_h(y, \mathbf{z}), \quad Q_h(\cdot, \mathbf{z}) = E\{w(\mathbf{Z}^0, \mathbf{z}, h)d^2(Y, \cdot)\}. \quad (8)$$

Here

$$w(\mathbf{Z}^0, \mathbf{z}, h) = \frac{1}{\mu_0 - \mu_1^{\top} \mu_2^{-1} \mu_1} K_h(\mathbf{Z}^0 - \mathbf{z}) \{1 - \mu_1^{\top} \mu_2^{-1} (\mathbf{Z}^0 - \mathbf{z})\},$$

where  $\mu_j = E\{K_h(\mathbf{Z}^0 - \mathbf{z})(\mathbf{Z}^0 - \mathbf{z})^{\oplus j}\}$  for  $j = 0, 1, 2$ . For an i.i.d. sample  $\{(\mathbf{Z}_i^0, Y_i)\}_{i=1}^n$ , the corresponding empirical version is

$$\tilde{v}_h(\mathbf{z}) = \arg \min_{y \in \Omega} \tilde{Q}_h(y, \mathbf{z}), \quad \tilde{Q}_h(\cdot, \mathbf{z}) = \frac{1}{n} \sum_{i=1}^n \tilde{w}(\mathbf{Z}_i^0, \mathbf{z}, h) d^2(Y_i, \cdot). \quad (9)$$

Here

$$\tilde{w}(\mathbf{Z}_i^0, \mathbf{z}, h) = \frac{1}{\tilde{\mu}_0 - \tilde{\mu}_1^\top \tilde{\mu}_2^{-1} \tilde{\mu}_1} K_h(\mathbf{Z}_i^0 - \mathbf{z}) \{1 - \tilde{\mu}_1^\top \tilde{\mu}_2^{-1} (\mathbf{Z}_i^0 - \mathbf{z})\}, \quad (10)$$

where  $\tilde{\mu}_j = n^{-1} \sum_{i=1}^n K_h(\mathbf{Z}_i^0 - \mathbf{z})(\mathbf{Z}_i^0 - \mathbf{z})^{\oplus j}$  for  $j = 0, 1, 2$ .

### 3 Methodology

Consider a totally bounded metric space  $(\Omega, d)$  with distance  $d : \Omega \times \Omega \mapsto [0, \infty)$ , and let  $\mathcal{M} \subset \Omega$  be a manifold isomorphic to a subspace of the Euclidean space  $\mathbb{R}^r$ . Let  $(\mathbf{X}, Y)$  be a random pair in  $\mathbb{R}^p \times \mathcal{M}$ , where  $\mathbf{X}$ , without loss of generality, is assumed to reside in the unit hypercube  $[0, 1]^p$ . Suppose  $\{(\mathbf{X}_i, Y_i)\}_{i=1}^n$  are  $n$  independent realizations of  $(\mathbf{X}, Y)$ . Let  $r$  be the intrinsic dimension of the manifold  $\mathcal{M}$ . There exists a bijective representation map of the manifold  $\mathcal{M}$ :

$$\psi : \mathcal{M} \mapsto \mathbb{R}^r. \quad (11)$$

Algorithms such as ISOMAP (Tenenbaum et al., 2000), locally linear embedding (Roweis and Saul, 2000), Laplacian eigenmaps (Belkin and Niyogi, 2003), or diffusion maps (Coifman and Lafon, 2006) are commonly employed to estimate the representation map  $\psi$ . Here we choose the ISOMAP algorithm; see Tenenbaum et al. (2000) for more details. The manifold representation is useful across many scenarios, for example when one has latent parametric families of probability distributions or stochastic block models for networks, where the low-dimensional manifold closely aligns with the parameters of the underlying model (Dubey et al., 2024).

We propose a unified framework, the deep Fréchet regression (DFR), to model the relationship between the metric-space valued response  $Y$  and a possibly high-dimensional multivariate predictor  $\mathbf{X}$ , as summarized in Figure 1.

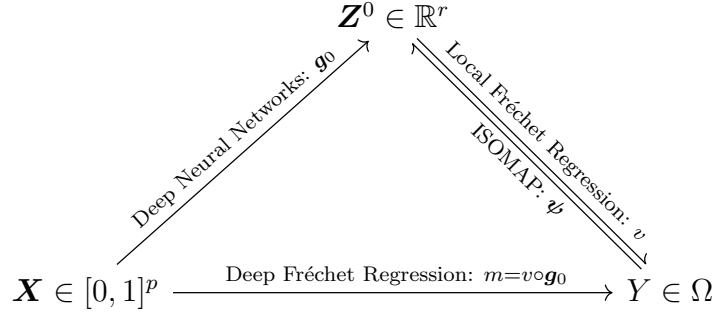


Figure 1: Schematic diagram for the deep Fréchet regression  $m = v \circ \mathbf{g}_0$ , where  $\mathbf{Z}^0 = \boldsymbol{\psi}(Y)$  denotes the low-dimensional representation of the metric-space valued response  $Y$ ,  $v$  the local Fréchet regression and  $\mathbf{g}_0$  the deep neural networks, one for each coordinate.

The regression function

$$m = v \circ \mathbf{g}_0 : [0, 1]^p \mapsto \Omega \quad (12)$$

exhibits a composite structure, where  $\mathbf{g}_0 = (g_{01}, \dots, g_{0r})^\top$  and  $v$  correspond to nonparametric regression using DNNs and local Fréchet regression, respectively. When the intrinsic dimension is  $r > 1$ , we fit one DNN for each coordinate. The proposed framework includes the ISOMAP representation  $\boldsymbol{\psi}$  which however is not known and must be estimated from the data, yielding  $\hat{\boldsymbol{\psi}}$ . We postulate that the manifold can be well identified at the sample points through the ISOMAP algorithm.

(I1) Consider  $\mathbf{Z}_i^0 = (Z_{i1}^0, \dots, Z_{ir}^0)^\top = \boldsymbol{\psi}(Y_i)$  and  $\mathbf{Z}_i = (Z_{i1}, \dots, Z_{ir})^\top = \hat{\boldsymbol{\psi}}(Y_i)$ . For each  $j = 1, \dots, r$ , there exists a function  $\pi_j : [0, 1]^{p \times n} \mapsto \mathbb{R}$  such that

$$Z_{ij} - Z_{ij}^0 = \pi_j(\mathbf{X}_1, \dots, \mathbf{X}_n)(\epsilon_{ij} + u_{nj}), \quad i = 1, \dots, n,$$

where the bias  $u_{nj} \rightarrow 0$  as  $n \rightarrow \infty$ , and  $\{\epsilon_{ij}\}_{i=1}^n$  are i.i.d. (mean zero) sub-Gaussian random variables with parameter 1 and independent of  $\{\mathbf{X}_i\}_{i=1}^n$ , i.e.,  $P(|\epsilon_{ij}| \geq t) \leq 2 \exp\{-t^2\}$ . Furthermore, there exists a constant  $C_{\pi_j}$  such that

$$C_{\pi_j} = \sup_{\{\mathbf{x}_1, \dots, \mathbf{x}_n\}} |\pi_j(\mathbf{x}_1, \dots, \mathbf{x}_n)| < \infty.$$

Assumption (II) is not overly restrictive as it allows for dependence between the estimated low-dimensional representations  $Z_{ij}$  and includes potential bias  $u_{nj}$  that may be induced by the ISOMAP algorithm. The dependence among  $Z_{ij}$  across different  $i$  is quantified by  $\pi_j$  with an upper bound  $C_{\pi_j}$  that is specific to each coordinate. This assumption aligns with similar considerations made in Kurisu et al. (2023) when employing DNNs to analyze time series data. The sub-Gaussian noise  $\epsilon_{ij}$  reflects randomness associated with the manifold estimation process.

We employ DNNs that take the observed predictors  $\mathbf{X}_i$  as input and produce the estimated low-dimensional representations  $\mathbf{Z}_i$  as output. For each  $j = 1, \dots, r$ , by Assumption (II) and the fact that  $Z_{ij}^0 = g_{0j}(\mathbf{X}_i)$  we may model the relationship between  $Z_{ij}$  and  $\mathbf{X}_i$  as

$$Z_{ij} = g_{0j}(\mathbf{X}_i) + \pi_j(\mathbf{X}_1, \dots, \mathbf{X}_n)(\epsilon_{ij} + u_{nj}). \quad (13)$$

Unlike the prevalent focus on independent Gaussian/sub-Gaussian noise without bias in the existing literature on DNNs (Bauer and Kohler, 2019; Schmidt-Hieber, 2020; Kohler and Langer, 2021), the noise  $\pi_j(\mathbf{X}_1, \dots, \mathbf{X}_n)(\epsilon_{ij} + u_{nj})$  considered in (13) exhibits dependence across different  $i$  and is accompanied by a vanishing bias  $u_{nj}$ , characterized by the randomness of a sub-Gaussian variable. Such generalizations necessitate a nontrivial expansion of the current theoretical framework for DNNs (Schmidt-Hieber, 2020); this extension is provided below as Theorem 1. The estimation of  $g_{0j}$  is performed by minimizing the empirical risk

$$\hat{g}_j = \arg \min_{g \in \mathcal{G}} \frac{1}{n} \sum_{i=1}^n \{Z_{ij} - g(\mathbf{X}_i)\}^2. \quad (14)$$

The proposed framework also deploys local Fréchet regression using the fitted value of DNNs  $\hat{\mathbf{Z}}_i = \hat{\mathbf{g}}(\mathbf{X}_i) = \{\hat{g}_1(\mathbf{X}_i), \dots, \hat{g}_r(\mathbf{X}_i)\}^\top$  in lieu of the unobservable  $\mathbf{Z}_i^0$  as predictors.

---

**Algorithm 1:** Deep Fréchet Regression

---

**Input:** data  $\{(\mathbf{X}_i, Y_i)\}_{i=1}^n$ , and a new predictor level  $\mathbf{X}$ .

**Output:** prediction  $\hat{m}(\mathbf{X})$ .

1 ISOMAP:

$\{\hat{\boldsymbol{\psi}}(Y_i)\}_{i=1}^n \leftarrow$  estimated low-dimensional representations of  $\{Y_i\}_{i=1}^n$ ,

and denote  $\hat{\boldsymbol{\psi}}(Y_i)$  by  $\mathbf{Z}_i = (Z_{i1}, \dots, Z_{ir})^\top$ ;

2 DNNs: for  $j = 1, \dots, r$ ,

$$\hat{g}_j \leftarrow \arg \min_{g \in \mathcal{G}} \frac{1}{n} \sum_{i=1}^n \{Z_{ij} - g(\mathbf{X}_i)\}^2,$$

where  $\hat{g}_j$  is the  $j$ th deep neural network trained using sample  $\{(\mathbf{X}_i, Z_{ij})\}_{i=1}^n$ ;

3  $\{\hat{\mathbf{Z}}_i\}_{i=1}^n \leftarrow \{(\hat{g}_1(\mathbf{X}_i), \dots, \hat{g}_r(\mathbf{X}_i))^\top\}_{i=1}^n$ ;

4 LFR:

$$\hat{m}(\mathbf{X}) = \hat{v}_h \circ \hat{\mathbf{g}}(\mathbf{X}) = \hat{v}_h(\hat{\mathbf{Z}}) \leftarrow \arg \min_{y \in \Omega} \frac{1}{n} \sum_{i=1}^n \hat{w}(\hat{\mathbf{Z}}_i, \hat{\mathbf{Z}}, h) d^2(Y_i, y),$$

where  $\hat{\mathbf{Z}} = \hat{\mathbf{g}}(\mathbf{X}) = (\hat{g}_1(\mathbf{X}), \dots, \hat{g}_r(\mathbf{X}))^\top$ .

---

This leads to an errors-in-variables version of local Fréchet regression,

$$\hat{v}_h(\mathbf{z}) = \arg \min_{y \in \Omega} \hat{Q}_h(y, \mathbf{z}), \quad \hat{Q}_h(\cdot, \mathbf{z}) = \frac{1}{n} \sum_{i=1}^n \hat{w}(\hat{\mathbf{Z}}_i, \mathbf{z}, h) d^2(Y_i, \cdot), \quad (15)$$

where

$$\hat{w}(\hat{\mathbf{Z}}_i, \mathbf{z}, h) = \frac{1}{\hat{\mu}_0 - \hat{\mu}_1^\top \hat{\mu}_2^{-1} \hat{\mu}_1} K_h(\hat{\mathbf{Z}}_i - \mathbf{z}) \{1 - \hat{\mu}_1^\top \hat{\mu}_2^{-1} (\hat{\mathbf{Z}}_i - \mathbf{z})\}, \quad (16)$$

with  $\hat{\mu}_j = n^{-1} \sum_{i=1}^n K_h(\hat{\mathbf{Z}}_i - \mathbf{z}) (\hat{\mathbf{Z}}_i - \mathbf{z})^{\oplus j}$  for  $j = 0, 1, 2$ .

Consequently, the regression function  $m$  as per (12), relating the predictor  $\mathbf{X}$  to the metric-space valued response  $Y$ , is estimated as

$$\hat{m} = \hat{v}_h \circ \hat{\mathbf{g}} \quad (17)$$

with  $\hat{v}_h$  and  $\hat{\mathbf{g}} = (\hat{g}_1, \dots, \hat{g}_r)^\top$  defined in (14) and (15). This comprehensive framework empowers us to effectively handle potentially high-dimensional predictors while simultaneously addressing the inherent complexities associated with metric-space valued responses. Further details are provided in Algorithm 1.

## 4 Asymptotic Properties

We first derive the convergence rate of DNN estimates (14), extending the existing theoretical framework for DNNs to accommodate dependent noise and bias. We then delve into the convergence rate of the local Fréchet regression estimate (15), considering multivariate predictors contaminated by errors induced by DNNs. Finally, the convergence rate of the deep Fréchet regression estimate as per (17) is established by combining the convergence rates of DNNs and local Fréchet regression. For DNN, we require (D1) and the following common assumption (Schmidt-Hieber, 2020; Kohler and Langer, 2021; Zhong et al., 2022).

(D2) The target function  $g_{0j}$  belongs to the Hölder class  $\mathcal{H}(q, \boldsymbol{\beta}, \mathbf{d}, \tilde{\mathbf{d}}, M)$  defined in (4) for  $j = 1, \dots, r$ .

Assumption (D2) states that the spaces of  $g_{0j}$  is the Hölder class  $\mathcal{H}(q, \boldsymbol{\beta}, \mathbf{d}, \tilde{\mathbf{d}}, M)$  which encompasses a rich class of smooth functions (Schmidt-Hieber, 2020; Kohler and Langer, 2021); see Section 2.2 for more details. The following result formalizes the convergence rate of DNN estimates (14).

**Theorem 1.** *Consider the nonparametric regression model (13). Under (I1), (D1) and (D2), for any  $i = 1, \dots, n$  and  $j = 1, \dots, r$ , there exists an estimator  $\hat{g}_j$  in (14) such that*

$$E[\{\hat{g}_j(\mathbf{X}_i) - g_{0j}(\mathbf{X}_i)\}^2] = O(\kappa_n^2 \log^3 n + |u_{nj}|)$$

and

$$E[\{\hat{g}_j(\mathbf{X}) - g_{0j}(\mathbf{X})\}^2] = O(\kappa_n^2 \log^3 n + |u_{nj}|)$$

where  $\mathbf{X}$  is a new realization of the predictor that is independent of the sample  $\{(\mathbf{X}_i, Y_i)\}_{i=1}^n$  and  $\kappa_n$  is defined in (6). It immediately follows that

$$E(\|\hat{\mathbf{Z}}_i - \mathbf{Z}_i^0\|^2) = O(\kappa_n^2 \log^3 n + u_n^2)$$

and

$$E(\|\hat{\mathbf{Z}} - \mathbf{Z}^0\|^2) = O(\kappa_n^2 \log^3 n + u_n^2),$$

where  $\hat{\mathbf{Z}} = (\hat{g}_1(\mathbf{X}), \dots, \hat{g}_r(\mathbf{X}))^\top$ ,  $\mathbf{Z}^0 = (g_{01}(\mathbf{X}), \dots, g_{0r}(\mathbf{X}))^\top$ ,  $u_n^2 = \max_{j=1, \dots, r} |u_{nj}|$  and  $g_{0j}$  are the components of  $\mathbf{g}_0$  as defined in (12).

All proofs are provided in the Supplementary Material. In contrast to the prevailing emphasis on DNNs with independent Gaussian/sub-Gaussian noise, Theorem 1 establishes the convergence rate of DNNs in the presence of dependent sub-Gaussian noise coupled with vanishing bias. This extension may also be useful for other work in the area of DNN. Note that the convergence rates in Theorem 1 depend on the bias term  $u_{nj}$ , smoothness  $\beta$ , and intrinsic dimension  $\tilde{\mathbf{d}}$  of functions  $g_{0j}$  as per (4), rather than the predictor dimension  $p$ . As a result, the proposed method can circumvent the curse of dimensionality, exhibiting a faster convergence rate particularly when the intrinsic dimension  $\tilde{\mathbf{d}}$  remains relatively low. For instance, disregarding the bias term momentarily, consider the true function  $g_{0j}$  structured in (5). For such a target function traditional smoothing methods are fraught with a slow convergence rate of order  $n^{-\frac{2}{p+4}} = n^{-\frac{1}{6}}$ , whereas the proposed DNN approach has a convergence rate of order  $n^{-\frac{2}{5}} \log^{3/2} n$ , reaching the optimal one-dimensional nonparametric regression convergence rate up to a polylogarithmic factor. This accelerated convergence rate effectively mitigates the curse of dimensionality inherent in nonparametric regression.

Next, we show the convergence rate for errors-in-variables multivariate local Fréchet regression, for which we require the following assumptions.

(L1) The minimizers  $v(\mathbf{z})$ ,  $v_h(\mathbf{z})$ ,  $\tilde{v}_h(\mathbf{z})$  and  $\hat{v}_h(\mathbf{z})$  for local Fréchet regression as per (7), (8), (9), and (15) exist and are unique, the last two almost surely. Additionally, for any  $\varepsilon > 0$ ,

- (i)  $\inf_{d\{v(\mathbf{z}), y\} > \varepsilon} [Q(y, \mathbf{z}) - Q\{v(\mathbf{z}), \mathbf{z}\}] > 0$ ,
- (ii)  $\liminf_{h \rightarrow 0} \inf_{d\{v_h(\mathbf{z}), y\} > \varepsilon} [Q_h(y, \mathbf{z}) - Q_h\{v_h(\mathbf{z}), \mathbf{z}\}] > 0$ ,
- (iii)  $P(\inf_{d\{\tilde{v}_h(\mathbf{z}), y\} > \varepsilon} [\tilde{Q}_h(y, \mathbf{z}) - \tilde{Q}_h\{\tilde{v}_h(\mathbf{z}), \mathbf{z}\}] > 0) \rightarrow 1$ ,
- (iv)  $P(\inf_{d\{\hat{v}_h(\mathbf{z}), y\} > \varepsilon} [\hat{Q}_h(y, \mathbf{z}) - \hat{Q}_h\{\hat{v}_h(\mathbf{z}), \mathbf{z}\}] > 0) \rightarrow 1$ .

(L2) Let  $B_\delta(y) \subset \Omega$  be the ball of radius  $\delta$  centered at  $y$  and  $N\{\varepsilon, B_\delta(y), d\}$  be its covering number using balls of size  $\varepsilon$  (see Definition 1 in Supplementary Material S.1). Then for any  $y \in \Omega$ ,

$$\int_0^1 [1 + \log N\{\delta\varepsilon, B_\delta(y), d\}]^{1/2} d\varepsilon = O(1) \quad \text{as } \delta \rightarrow 0.$$

(L3) There exists  $\eta_1, \eta_2, \eta_3 > 0$ ,  $C_1, C_2, C_3 > 0$  and  $\gamma_1, \gamma_2, \gamma_3 > 1$  such that

- (i)  $\inf_{d\{v(\mathbf{z}), y\} < \eta_1} [Q(y, \mathbf{z}) - Q\{v(\mathbf{z}), \mathbf{z}\} - C_1 d\{v(\mathbf{z}), y\}^{\gamma_1}] \geq 0$ ,
- (ii)  $\liminf_{h \rightarrow 0} \inf_{d\{v_h(\mathbf{z}), y\} < \eta_2} [Q_h(y, \mathbf{z}) - Q_h\{v_h(\mathbf{z}), \mathbf{z}\} - C_2 d\{v_h(\mathbf{z}), y\}^{\gamma_2}] \geq 0$ ,
- (iii)  $P(\inf_{d\{\tilde{v}_h(\mathbf{z}), y\} < \eta_3} [\tilde{Q}_h(y, \mathbf{z}) - \tilde{Q}_h\{\tilde{v}_h(\mathbf{z}), \mathbf{z}\} - C_3 d\{\tilde{v}_h(\mathbf{z}), y\}^{\gamma_3}] \geq 0) \rightarrow 1$ ,

Assumption (L1) is a standard requirement to ensure the consistency of M-estimators, as outlined by Van der Vaart and Wellner (2023). We note that the existence and uniqueness of the minimizers in (L1) is guaranteed for the case of Hadamard spaces, the curvature of which is bounded above by 0 (Sturm, 2003). Assumption (L2) entails conditions on



the metric entropy of  $\Omega$  to control its size. In Proposition 1, it constrains the bracketing integral used to derive the tail bound, following Theorem 2.14.16 in [Van der Vaart and Wellner \(2023\)](#). The curvature assumption in (iii) regulates the behavior of  $(Q_h - Q)$ ,  $(\tilde{Q}_h - Q_h)$ , and  $(\hat{Q}_h - \tilde{Q}_h)$  near their minima, which makes it possible to derive convergence rates. These assumptions stem from empirical process theory and are frequently employed in the literature concerning statistical analysis for metric-space valued data ([Petersen and Müller, 2019](#); [Schötz, 2022](#); [Chen and Müller, 2022](#); [Zhang et al., 2023](#)).

We now provide some statistically relevant examples of metric spaces, for which we demonstrate in Section S.2 of the Supplementary Material that these metric spaces satisfy Assumptions (L1)–(iii); see Propositions 3, 4 and 5.

**Example 1.** *Let  $\Omega$  be the space of probability distributions on a closed interval of  $\mathbb{R}$  with finite second moments, equipped with the Wasserstein metric  $d_W$  where*

$$d_W^2(\mu, \nu) = \int_0^1 \{F_\mu^{-1}(p) - F_\nu^{-1}(p)\}^2 dp$$

*for any two probability distributions  $\mu, \nu \in \Omega$ . The Wasserstein space  $(\Omega, d_W)$  satisfies Assumptions (L1)–(iii) with  $\gamma_1 = \gamma_2 = \gamma_3 = 2$ .*

**Example 2.** *Let  $\Omega$  be the space of graph Laplacians of undirected weighted networks with a fixed number of nodes  $m$  and bounded edge weights equipped with the Frobenius metric  $d_F$ . The space  $(\Omega, d_F)$  satisfies Assumptions (L1)–(iii) with  $\gamma_1 = \gamma_2 = \gamma_3 = 2$ .*

**Example 3.** *Let  $\Omega$  be the space of  $m$ -dimensional covariance matrices with bounded variances or correlation matrices equipped with the Frobenius metric  $d_F$ . The space  $(\Omega, d_F)$  satisfies Assumptions (L1)–(iii) with  $\gamma_1 = \gamma_2 = \gamma_3 = 2$ .*

We next derive the convergence rate of multivariate local Fréchet regression, extending previous results for local Fréchet regression (9) with one-dimensional predictors. The

proof relies on M-estimation techniques arising from empirical process theory. The kernel and distributional assumptions (K1) and (P1) listed in the Appendix are standard for local regression. In the following,  $r$  is as in (11) the intrinsic dimension of the manifold representation (11).

**Proposition 1.** *If (K1), (P1), (L1) (i)–(ii) and (iii) (i)–(ii) hold, then*

$$d\{v_h(\mathbf{z}), v(\mathbf{z})\} = O(h^{2/(\gamma_1-1)}) \quad (18)$$

as  $h \rightarrow 0$ . If furthermore  $nh^r \rightarrow \infty$ , then

$$d\{\tilde{v}_h(\mathbf{z}), v_h(\mathbf{z})\} = O_p\{(nh^r)^{-1/\{2(\gamma_2-1)\}}\}. \quad (19)$$

In general, the convergence rates are determined by the local geometry near the minimum as quantified in (iii). For metric spaces in Examples 1, 2 and 3,  $\gamma_1 = \gamma_2 = 2$  and convergence rates of the bias and stochastic deviation are  $d\{v_h(\mathbf{z}), v(\mathbf{z})\} = O(h^2)$  and  $d\{\tilde{v}_h(\mathbf{z}), v_h(\mathbf{z})\} = O_p\{(nh^r)^{-1/2}\}$ , respectively. With  $h = n^{-1/(4+r)}$ , the multivariate local Fréchet regression estimate achieves the rate  $d\{\tilde{v}_h(\mathbf{z}), v(\mathbf{z})\} = O_p(n^{-2/(4+r)})$ , corresponding to the well-known optimal rate for standard local linear regression.

The low-dimensional representations  $\mathbf{Z}_i^0$  in (9) are unobservable, necessitating the use of (15) in practice, where the estimated representations  $\hat{\mathbf{Z}}_i$  obtained through DNNs are substituted. Consequently, errors are introduced in the predictors of local Fréchet regression, leading to the need to address the errors-in-variables problem. The following theorem characterizes the impact of these errors on the estimation.

**Proposition 2.** *Suppose (K1), (L1), (iii) hold. If  $\|\hat{\mathbf{Z}}_i - \mathbf{Z}_i^0\| = O_p(\zeta_n)$  for  $i = 1, \dots, n$ ,  $\|\hat{\mathbf{Z}} - \mathbf{Z}^0\| = O_p(\zeta_n)$ ,  $nh^r \rightarrow \infty$ , and  $h^{-r-2}\zeta_n \rightarrow 0$ , then it holds for  $\tilde{v}_h(\cdot)$  and  $\hat{v}_h(\cdot)$  as per (9) and (15) that*

$$d\{\hat{v}_h(\hat{\mathbf{Z}}), \tilde{v}_h(\mathbf{Z}^0)\} = O_p\{(h^{-r-1}\zeta_n)^{1/(\gamma_3-1)}\}. \quad (20)$$

For metric spaces in Examples 1, 2 and 3,  $\gamma_3 = 2$  and the convergence rate provided in Proposition 2 reduces to  $O_p\{(h^{-r-1}\zeta_n)\}$ . Combining Theorems 1 and Proposition 1 and 2, we have the following Theorem.

**Theorem 2.** *If (I1), (D1)–(D2), (K1), (P1), (L1)–(iii) hold and furthermore  $nh^r \rightarrow \infty$ ,  $h^{-r-2}\zeta_n \rightarrow 0$ , one has*

$$d\{\hat{m}(\mathbf{X}), m(\mathbf{X})\} = O_p\{h^{2/(\gamma_1-1)} + (nh^r)^{-1/\{2(\gamma_2-1)\}} + (h^{-r-1}\zeta_n)^{1/(\gamma_3-1)}\}, \quad (21)$$

where  $\mathbf{X}$  is a new predictor independent of the sample  $\{(\mathbf{X}_i, Y_i)\}_{i=1}^n$  and  $\zeta_n = \kappa_n \log^{3/2} n + u_n$ .

The initial two terms  $h^{2/(\gamma_1-1)}$ ,  $(nh^r)^{-1/\{2(\gamma_2-1)\}}$  in Theorem 2 give the convergence rate of multivariate local Fréchet regression, as outlined in Proposition 1, representing the optimal rate when  $\mathbf{Z}_i^0$ ,  $\boldsymbol{\psi}$ , and  $\mathbf{g}_0$  are known. The final term,  $(h^{-r-1}\zeta_n)^{1/(\gamma_3-1)}$ , originates from Theorem 1 and Proposition 2, reflecting errors introduced during the estimation of low-dimensional representations of metric-space valued responses (ISOMAP), DNNs, and the subsequent errors-in-variables problem.

If one assumes  $E\{\sup_{i=1,\dots,n}(\hat{\mathbf{Z}}_i - \mathbf{Z}_i^0)^2\} = O(\tau_n^2)$ , the dependence of the convergence rate presented in Proposition 2 on the intrinsic dimension of metric-space valued responses  $r$  would vanish. Specifically, the convergence rate in Proposition 2 would be further improved to  $(h^{-1}\tau_n)^{1/(\gamma_3-1)}$ , leading to an enhanced convergence rate of the proposed model as  $h^{2/(\gamma_1-1)} + (nh^r)^{-1/2(\gamma_2-1)} + (h^{-1}\tau_n)^{1/(\gamma_3-1)}$ . The proof is provided in the Supplementary Material S.7. While the primary focus of the current work is to devise a general framework for handling multivariate predictors and metric-space valued responses, it would be intriguing for future work to derive such a supremum rate for DNNs when dealing with dependent sub-Gaussian noise coupled with bias.

## 5 Implementation and Simulations

### 5.1 Implementation details

The optimization problem in (14) was addressed within *Pytorch* framework, where we opted for the Adam optimizer (Kingma and Ba, 2014), a widely used choice in deep learning known for its robust performance across diverse models and datasets. The weight matrices  $W_l$  and shift vectors  $\mathbf{b}_l$  of the function  $g \in \mathcal{G}$  as per (3) were initialized using the default random initialization provided by *Pytorch*.

Manifold learning (ISOMAP) and DNNs involve tuning parameters such as the number of nearest neighbors  $k$  in the Dijkstra algorithm (Dijkstra, 1959), the number of hidden layers  $L$ , the number of neurons  $p_l$  in each hidden layer, dropout rate, and learning rate. For simplicity, we maintained the same number of neurons in each hidden layer. The dropout rate (Srivastava et al., 2014) is the rate of randomly excluding neurons during training. The learning rate (Goodfellow et al., 2016) determines the step size for gradient descent in the Adam algorithm. Tuning these parameters can be accomplished through a grid search, assessing empirical risk over a held-out validation set after each training iteration. We set aside 20% of the training set as the validation set in each run. The training process stops when the empirical risk on the validation set ceases to reliably improve.

### 5.2 Simulations for probability distributions

To assess the performance of the proposed model, we report the results of simulations for various settings. The random objects we consider first are univariate probability distributions equipped with the Wasserstein metric; see Example 1. The Wasserstein space is a geodesic metric space related to optimal transport (Villani, 2003) and is increasingly

applied in various research domains, including population pyramids (Bigot et al., 2017; Delicado, 2011), financial returns (Zhang et al., 2022), and multi-cohort studies (Zhou and Müller, 2023), among others (Petersen et al., 2022). Additional simulations for networks can be found in Supplementary Material S.8. Despite the simulated networks not residing on a 2-dimensional manifold, the proposed model exhibits remarkable robustness as the sample size increases.

Consider the true regression function, represented as a quantile function, to be

$$m(\mathbf{X}) = E(\eta|\mathbf{X}) + E(\sigma|\mathbf{X})\Phi^{-1}(\cdot),$$

which corresponds to a Gaussian distribution with mean and standard deviation depending on  $\mathbf{X}$ . The distribution parameters of  $m(\mathbf{X})$  are generated conditionally on  $\mathbf{X}$ , where the mean  $\eta$  and the standard deviation  $\sigma$  are assumed to follow a normal distribution and a Gamma distribution, respectively.

We consider sample sizes  $n = 100, 200, 500, 1000$ , with  $Q = 500$  Monte Carlo runs. In each Monte Carlo run, predictors  $\mathbf{X}_i \in \mathbb{R}^9$ ,  $i = 1, \dots, n$ , are independently sampled as

$$X_{i1} \sim U(-1, 0), \quad X_{i2} \sim U(0, 1), \quad X_{i3} \sim U(1, 2)$$

$$X_{i4} \sim N(0, 1), \quad X_{i5} \sim N(-10, 3), \quad X_{i6} \sim N(10, 3)$$

$$X_{i7} \sim \text{Bernoulli}(0.6), \quad X_{i8} \sim \text{Bernoulli}(0.7), \quad X_{i9} \sim \text{Bernoulli}(0.3).$$

For each  $i$ , the mean and standard deviation of the Gaussian distribution are generated conditionally on  $\mathbf{X}_i$  as

$$\eta_i|\mathbf{X}_i \sim N(\mu, 0.5^2), \sigma_i|\mathbf{X}_i \sim \text{Gamma}(\theta^2, \theta^{-1}) \text{ where}$$

$$\mu = 3X_{i8}\{\sin(\pi X_{i1}) + \cos(\pi X_{i2})\} + X_{i7}(5X_{i4}^2 + X_{i5}),$$

$$\theta = [3 + 0.5X_{i8}\{\sin(\pi X_{i1}) + \cos(\pi X_{i2})\} + X_{i7}[5X_{i4}^2 + X_{i5}]].$$

The corresponding distributional response is then constructed as  $Y_i = \eta_i + \sigma_i \Phi^{-1}$ .

To simulate practical scenarios where direct observations of probability distributions are not available, but rather independent data samples generated by the corresponding distribution are obtained, we independently sample 100 observations  $\{y_{ij}\}_{j=1}^{100}$  from each distributional response  $Y_i$ . Consequently, one must initially estimate the distributional response  $Y_i$  from the random sample  $\{y_{ij}\}_{j=1}^{100}$ , introducing a bias to the regression model. This practical consideration aligns with prior research (Zhou and Müller, 2023), which addresses the issue by adopting the empirical measure in place of the unobservable distributional response  $Y_i$ . For the implementation of local Fréchet regression using empirical measures, we follow the algorithm outlined in Zhou and Müller (2023). The bandwidths for the local Fréchet regression in each Monte Carlo run are chosen as 10% of the range of the intermediate estimates  $\hat{\mathbf{Z}}_i = \hat{\mathbf{g}}(\mathbf{X}_i)$ .

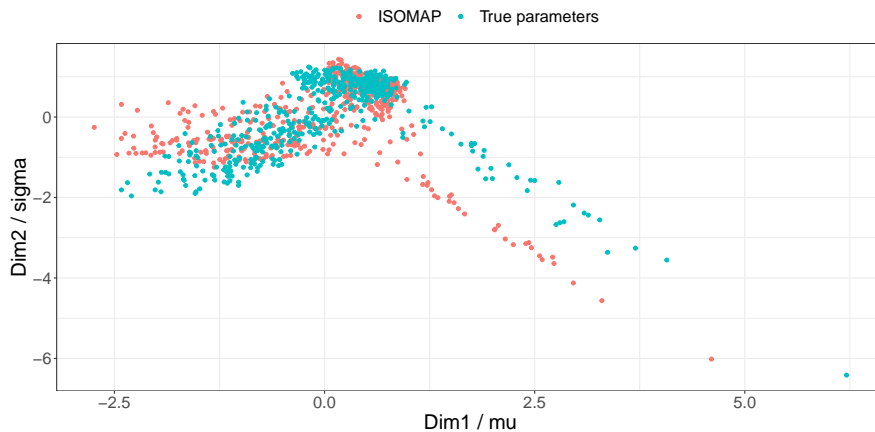
For the  $q$ th Monte Carlo run out of  $Q = 500$  runs, with  $\hat{m}_q(\cdot)$  denoting the fitted regression function, the quality of the estimation is quantified by the mean squared prediction error (MSPE),

$$\text{MSPE}_q = \frac{1}{100} \sum_{i=1}^{100} d_{\mathcal{W}}^2\{\hat{m}_q(\mathbf{X}_i^{\text{test}}), m(\mathbf{X}_i^{\text{test}})\},$$

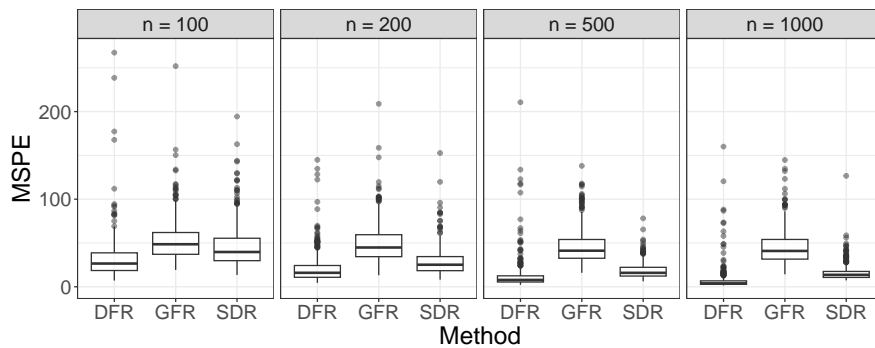
where  $\{\mathbf{X}_i^{\text{test}}\}_{i=1}^{100}$  denote out-of-sample predictors and the metric  $d_{\mathcal{W}}$  is the Wasserstein metric for probability distributions. The average quality of the estimation over the  $Q = 500$  Monte Carlo runs is quantified by the average mean squared prediction error (AMSPE)

$$\text{AMSPE} = \frac{1}{Q} \sum_{q=1}^Q \text{MSPE}_q.$$

To assess the validity of the manifold assumption, Figure 2(a) presents a scatter plot depicting the two-dimensional representations of distributional responses  $\{Y_i\}_{i=1}^n$  alongside their true parameters (mean and standard deviation) for a sample size of  $n = 500$ . The plot reveals a distinctive horseshoe shape in the two-dimensional representations, implying



(a)



(b)

Figure 2: (a) Two-dimensional representations of probability distributions  $\{Y_i\}_{i=1}^n$  using ISOMAP, along with their true parameters (mean and standard deviation) for sample size  $n = 500$ . (b) Boxplot of mean squared prediction errors for  $Q = 500$  Monte Carlo runs using deep Fréchet regression (the proposed method), global Fréchet regression (Petersen and Müller, 2019) and sufficient dimension reduction (Zhang et al., 2023).

that the distributional responses adhere to a lower-dimensional manifold. Intriguingly, the two-dimensional representations closely align with the two-dimensional parameters of the distributional responses. This observation suggests that for distributional responses ISOMAP effectively identifies suitable low-dimensional representations corresponding to the latent parameter space.

We conduct comparisons with global Fréchet regression (GFR) (Petersen and Müller, 2019) and local Fréchet regression with sufficient dimension reduction (SDR) (Zhang et al., 2023). Figure 2(b) summarizes MSPEs for all Monte Carlo runs and various sample sizes

Table 1: Average mean squared prediction error of deep Fréchet regression (the proposed method), global Fréchet regression (Petersen and Müller, 2019) and sufficient dimension reduction (Zhang et al., 2023) for distributional responses.

n	DFR	GFR	SDR
100	34.288	52.947	45.215
200	21.464	49.685	28.390
500	12.190	45.836	19.122
1000	9.305	46.076	15.8875

using the proposed model, GFR and SDR. The MSPE decreases with increasing sample size, indicating the convergence of the proposed model to the target. Notably, the proposed model exhibits superior performance over GFR and SDR across all sample sizes, including the case of  $n = 100$ . In Table 1, we present the AMSPE for different sample sizes. The proposed model (DFR) is seen to fare best across different methods. Despite the conventional need for large sample sizes in the performance of deep neural networks, the proposed model surprisingly demonstrates robustness for small sample sizes, potentially owing to its flexibility in accommodating complex regression relationships.

## 6 Data Application

Yellow and green taxi trip records in New York City (NYC), including pick-up and drop-off dates, locations, trip distances, payment methods, and passenger counts, are available at <https://www.nyc.gov/site/tlc/about/tlc-trip-record-data.page>. Additionally, we collect NYC weather history, including daily average temperature, humidity, wind speed, pressure, and total precipitation from <https://www.wunderground.com/history/daily/us/ny/new-york-city/KLGA/date>. The objective is to predict transport networks constructed from taxi trip records using relevant predictors. Given the potential influence of weather conditions on travel plans, the variability in travel patterns across different days of



Table 2: Predictors of New York taxi network data.

Category	Variables	Explanation
Weather	1. Temp	daily average temperature
	2. Humidity	daily average humidity
	3. Wind	daily average windspeed
	4. Pressure	daily average barometric pressure
	5. Precipitation	daily total precipitation
Day	6. Mon to Thur	indicator for Monday to Thursday
	7. Sun or Holiday	indicator for Sunday or holidays
Trip	8. Passenger Count	daily average number of passengers
	9. Trip Distance	daily average trip distance
	10. Fare Amount	daily average fare amount
	11. Tip Amount	daily average tip amount
	12. Tolls Amount	daily average tip amount
	13. Credit Card	average of credit card indicators for the type of payment
	14. Cash	average of cash indicators for the type of payment
	15. Dispute	average of dispute indicators for the type of payment

the week, and the impact of daily trip features on the taxi system, we construct a fifteen-dimensional predictor set including daily weather information, indicators for days of the week or holiday, and daily trip features averaged over each day; see Table 2.

We analyze yellow taxi trip records in Manhattan, excluding islands, and divide the 66 taxi zones into 13 regions based on preprocessing procedures outlined in [Zhou and Müller \(2022\)](#). While [Zhou and Müller \(2022\)](#) focused on the effect of COVID-19 on the transport network, our study investigates the pre-COVID transport network. Therefore, we limit our analysis to a period of 1092 days from January 1, 2017, to December 31, 2019, excluding 3 outlier days. The main interest regarding these traffic records is the transport network that represents daily passenger movement between the 13 regions. To this end, we build daily undirected networks with nodes standing for the 13 regions and edge weights representing the number of passengers traveling between the regions. Each of these networks is uniquely

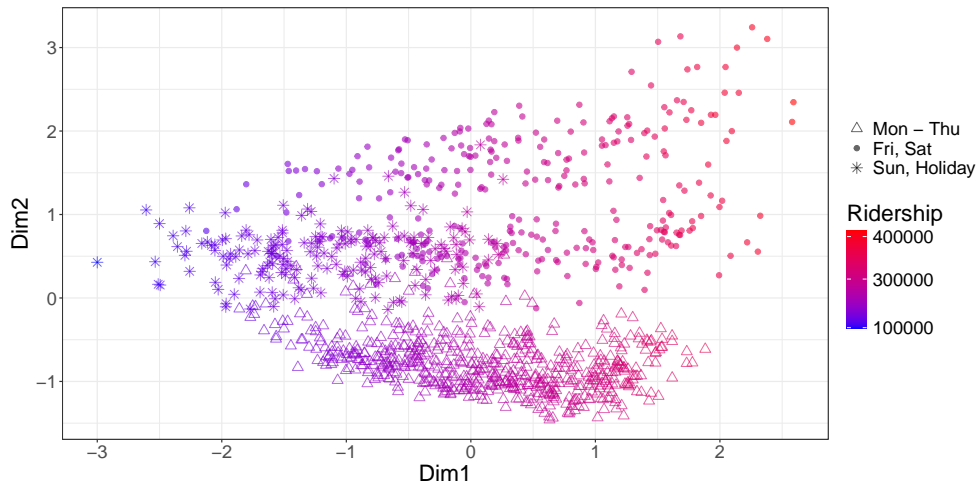


Figure 3: Two-dimensional representations of 1092 taxi networks using MDS with respect to the Frobenius metric.

associated with a  $13 \times 13$  graph Laplacian. The two-dimensional representations of 1092 graph Laplacians using MDS are shown in Figure 3 which suggest a clear separation among Monday to Thursday, Friday or Saturday, and Sunday or holiday in the second dimension. Additionally, as the first dimension increases, the total ridership also increases. The scatter plot exhibits a horseshoe shape, indicating that the manifold assumption is plausible within this context.

The proposed model was applied to model the relationship between daily graph Laplacians and the fifteen-dimensional predictors. The MSPE was calculated using 10-fold cross-validation, averaged over 100 runs. The proposed method achieves better prediction performance, resulting in a 46% and 55% improvement in prediction accuracy compared to GFR (Zhou and Müller, 2022) and SDR (Zhang et al., 2023), respectively. To further investigate the effect of daily total precipitation on taxi traffic, we predicted networks with varying total precipitation levels and fixed all other covariates at their median levels. Figure 4 shows the predicted networks at total precipitation levels of 0, 2, and 6 inches on Monday to Thursday, Friday or Saturday, and Sunday or holiday. We observed that edge weights

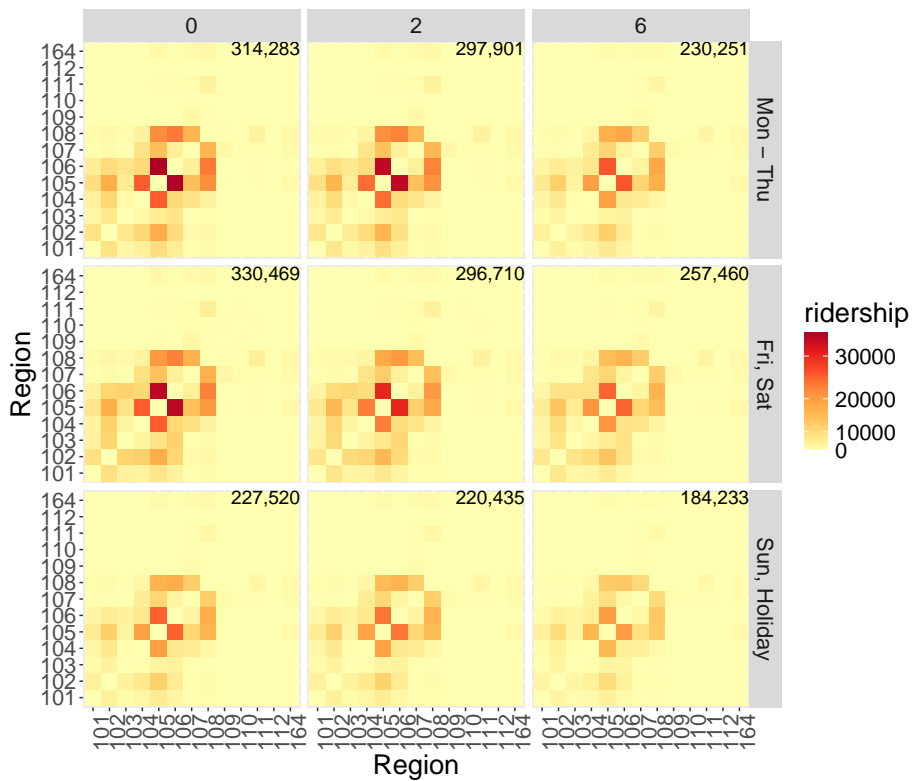


Figure 4: Predicted networks represented as heatmaps at different levels of total precipitation on Monday to Thursday, Friday or Saturday, and Sunday or holiday. The left, middle, and right columns show, respectively, the predicted networks at 0, 2, and 6 inches of total precipitation. The three rows depict the predicted networks on Monday to Thursday, Friday or Saturday, and Sunday or holiday, respectively. The value in the top right corner of each panel represents the total ridership of the entire transport network.

decrease on Sunday or holiday compared with those on Monday to Saturday, regardless of total precipitation levels. This suggests that more people tend to stay at home on Sunday and holiday. Across different precipitation levels, the taxi traffic from Monday to Thursday is more concentrated in areas 105, 106, 107, and 108, which are primarily residential areas with popular destinations such as Penn Station and Grand Central Terminal. Conversely, taxi traffic on Friday and Saturday is more diffuse, spreading into areas 102, 103, and 104, which are home to popular bars, restaurants, chain stores, and high-end art galleries and museums. As the total precipitation increases, taxi traffic decreases, irrespective of the day of the week. When the total precipitation reaches 6 inches, corresponding to a rainstorm,

the remaining taxi traffic for all three categories of days is primarily concentrated in areas 105, 106, 107, and 108. This may be related to unavoidable activities such as work-related events. However, discretionary travel plans, primarily observed in areas 102, 103, and 104, are more likely to be canceled due to adverse weather conditions.

## 7 Discussion

The proposed deep Fréchet regression model introduces a novel approach for analyzing metric-space responses using multivariate predictors. Extensive simulations and applications across diverse scenarios, including networks and probability distributions, highlight the versatility of the model. The proposed approach is flexible and requires no specific model assumptions. Key contributions include an in-depth exploration of the convergence rate of deep neural networks under dependent sub-Gaussian noise with bias and an extension of the scope of local Fréchet regression to handle multivariate predictors, including the convergence rate in an errors-in-variables regression framework. The proposed approach can be easily adapted to various manifold learning methods, such as locally linear embedding, Laplacian eigenmaps and diffusion maps.

A limitation lies in the assumption of the existence of a low-dimensional representation of random objects. However, our simulations and applications demonstrate the broad applicability of the proposed method, showcasing robust performance even when the intrinsic dimension of metric-space valued responses is not low. Open problems for future research include the supremum rate of DNN convergence when dealing with dependent sub-Gaussian noise with bias and the case of high-dimensional predictors.

# Acknowledgments

This research was supported in part by NSF grant DMS-2310450.

## Appendix A. Kernel and distributional assumptions

(K1) The  $r$ -dimensional kernel  $K(\cdot)$  satisfies  $\int_{\mathbb{R}^r} K(\mathbf{u})u_j^4 d\mathbf{u} < \infty$  and  $\int_{\mathbb{R}^r} K^2(\mathbf{u})u_j^6 d\mathbf{u} < \infty$  for  $j = 1, \dots, r$  and  $\mathbf{u} = (u_1, \dots, u_r)^\top$ , and is Lipschitz continuous with compact support  $[-1, 1]^r$ .

(P1) Both the marginal density  $f_{\mathbf{Z}^0}(\cdot)$  of  $\mathbf{Z}^0$  and the conditional densities  $f_{\mathbf{Z}^0|Y}(\cdot, y)$  of  $\mathbf{Z}^0$  given  $Y = y$  exist and are twice continuously differentiable, the latter for all  $y \in \Omega$ , and  $\sup_{\mathbf{z}, y} |(\partial^2 f_{\mathbf{Z}^0|Y} / \partial \mathbf{z}^2)(\mathbf{z}, y)| < \infty$ . In addition, for any open set  $U \subset \Omega$ ,  $\int_U dF_{Y|\mathbf{Z}^0}(\mathbf{z}, y)$  is continuous as a function of  $\mathbf{z}$ .

## References

- Anthony, M., P. L. Bartlett, and P. L. Bartlett (1999). *Neural Network Learning: Theoretical Foundations*, Volume 9. Cambridge University Press.
- Bauer, B. and M. Kohler (2019). On deep learning as a remedy for the curse of dimensionality in nonparametric regression. *Annals of Statistics* 47(4), 2261–2285.
- Belkin, M. and P. Niyogi (2003). Laplacian eigenmaps for dimensionality reduction and data representation. *Neural Computation* 15, 1373–1396.
- Bhattacharjee, S. and H.-G. Müller (2023). Single index Fréchet regression. *Annals of Statistics* 51(4), 1770–1798.

- Bigot, J., R. Gouet, T. Klein, and A. López (2017). Geodesic PCA in the Wasserstein space by convex PCA. *Annales de l'Institut Henri Poincaré B: Probability and Statistics* 53, 1–26.
- Bos, T. and J. Schmidt-Hieber (2023). A supervised deep learning method for nonparametric density estimation. *arXiv preprint arXiv:2306.10471*.
- Chen, D. and H.-G. Müller (2012). Nonlinear manifold representations for functional data. *Annals of Statistics* 40, 1–29.
- Chen, Y. and H.-G. Müller (2022). Uniform convergence of local Fréchet regression, with applications to locating extrema and time warping for metric-space valued trajectories. *Annals of Statistics* 50(3), 1573–1592.
- Chen, Y., Y. Zhou, H. Chen, A. Gajardo, J. Fan, Q. Zhong, P. Dubey, K. Han, S. Bhattacharjee, C. Zhu, S. I. Iao, P. Kundu, A. Petersen, and H.-G. Müller (2023). *frechet: Statistical Analysis for Random Objects and Non-Euclidean Data*. R package version 0.3.0.
- Coifman, R. R. and S. Lafon (2006). Diffusion maps. *Applied and Computational Harmonic Analysis* 21(1), 5–30.
- Delicado, P. (2011). Dimensionality reduction when data are density functions. *Computational Statistics & Data Analysis* 55, 401–420.
- Dijkstra, E. W. (1959). A note on two problems in connexion with graphs. *Numerische Mathematik* 1, 269–271.
- Dryden, I. L., A. Koloydenko, and D. Zhou (2009). Non-Euclidean statistics for covariance

- matrices, with applications to diffusion tensor imaging. *Annals of Applied Statistics* 3, 1102–1123.
- Dubey, P., Y. Chen, and H.-G. Müller (2024). Metric statistics: Exploration and inference for random objects with distance profiles. *Annals of Statistics* 52(2), 757–792.
- Fan, J. and I. Gijbels (1996). *Local Polynomial Modelling and its Applications*. London: Chapman & Hall.
- Faraway, J. J. (2014). Regression for non-Euclidean data using distance matrices. *Journal of Applied Statistics* 41, 2342–2357.
- Fréchet, M. (1948). Les éléments aléatoires de nature quelconque dans un espace distancié. *Annales de l’Institut Henri Poincaré* 10(4), 215–310.
- Ghojogh, B., M. Crowley, F. Karray, and A. Ghodsi (2023). *Elements of Dimensionality Reduction and Manifold Learning*. Springer New York.
- Goodfellow, I., Y. Bengio, and A. Courville (2016). *Deep Learning*. MIT Press.
- Han, S., J. Pool, J. Tran, and W. Dally (2015). Learning both weights and connections for efficient neural network. *Advances in Neural Information Processing Systems* 28.
- Hein, M. (2009). Robust Nonparametric Regression with Metric-Space valued Output. In *Advances in Neural Information Processing Systems*, pp. 718–726.
- Kingma, D. P. and J. Ba (2014). Adam: A method for stochastic optimization. *arXiv preprint arXiv:1412.6980*.
- Kohler, M. and S. Langer (2021). On the rate of convergence of fully connected deep neural network regression estimates. *Annals of Statistics* 49(4), 2231–2249.

- Kurusu, D., R. Fukami, and Y. Koike (2023). Adaptive deep learning for nonparametric time series regression. *Bernoulli*, just-accepted.
- LeCun, Y., Y. Bengio, and G. Hinton (2015). Deep learning. *Nature* 521(7553), 436–444.
- Müller, H.-G. (2016). Peter Hall, Functional Data Analysis and Random Objects. *Annals of Statistics* 44, 1867–1887.
- Nair, V. and G. E. Hinton (2010). Rectified linear units improve restricted Boltzmann machines. In *International Conference on Machine Learning*, pp. 807–814.
- Nye, T. M., X. Tang, G. Weyenberg, and R. Yoshida (2017). Principal component analysis and the locus of the Fréchet mean in the space of phylogenetic trees. *Biometrika* 104(4), 901–922.
- Petersen, A. and H.-G. Müller (2019). Fréchet regression for random objects with Euclidean predictors. *Annals of Statistics* 47(2), 691–719.
- Petersen, A., C. Zhang, and P. Kokoszka (2022). Modeling probability density functions as data objects. *Econometrics and Statistics* 21, 159–178.
- Roweis, S. T. and L. K. Saul (2000). Nonlinear dimensionality reduction by locally linear embedding. *Science* 290(5500), 2323–2326.
- Schmidt-Hieber, J. (2020). Nonparametric regression using deep neural networks with ReLU activation function. *Annals of Statistics* 48(4), 1875–1897.
- Schötz, C. (2022). Nonparametric regression in nonstandard spaces. *Electronic Journal of Statistics* 16(2), 4679–4741.
- Song, D. and K. Han (2023). Errors-in-variables Fréchet regression with low-rank covariate approximation. In *Advances in Neural Information Processing Systems*.



- Srinivas, S., A. Subramanya, and R. Venkatesh Babu (2017). Training sparse neural networks. In *Computer Vision and Pattern Recognition*, pp. 138–145.
- Srivastava, N., G. Hinton, A. Krizhevsky, I. Sutskever, and R. Salakhutdinov (2014). Dropout: a simple way to prevent neural networks from overfitting. *Journal of Machine Learning Research* 15(1), 1929–1958.
- Sturm, K.-T. (2003). Probability measures on metric spaces of nonpositive curvature. *Heat Kernels and Analysis on Manifolds, Graphs, and Metric Spaces (Paris, 2002)*. *Contemp. Math.*, 338. Amer. Math. Soc., Providence, RI 338, 357–390.
- Tenenbaum, J. B., V. De Silva, and J. C. Langford (2000). A global geometric framework for nonlinear dimensionality reduction. *Science* 290, 2319–2323.
- Tucker, D. C., Y. Wu, and H.-G. Müller (2023). Variable selection for global Fréchet regression. *Journal of the American Statistical Association* 118(542), 1023–1037.
- Van der Vaart, A. and J. Wellner (2023). *Weak Convergence and Empirical Processes: With Applications to Statistics*. Springer New York.
- Villani, C. (2003). *Topics in Optimal Transportation*. American Mathematical Society.
- Ying, C. and Z. Yu (2022). Fréchet sufficient dimension reduction for random objects. *Biometrika* 109(4), 975–992.
- Zhang, C., P. Kokoszka, and A. Petersen (2022). Wasserstein autoregressive models for density time series. *Journal of Time Series Analysis* 43(2), 30–52.
- Zhang, Q., L. Xue, and B. Li (2023). Dimension reduction for Fréchet regression. *Journal of the American Statistical Association* (just-accepted), 1–15.

Zhong, Q., J. Mueller, and J.-L. Wang (2022). Deep learning for the partially linear Cox model. *Annals of Statistics* 50(3), 1348–1375.

Zhou, Y. and H.-G. Müller (2022). Network regression with graph Laplacians. *Journal of Machine Learning Research* 23, 1–41.

Zhou, Y. and H.-G. Müller (2023). Wasserstein regression with empirical measures and density estimation for sparse data. *arXiv preprint arXiv:2308.12540*.

# Supplementary Material

## S.1 Additional Background

**Definition 1** (Covering number). *Let  $(\Omega, d)$  be a metric space. Let  $S \subseteq \Omega$  be a subset and  $\varepsilon > 0$ . The  $\varepsilon$ -covering number of  $S$ , denoted by  $N(\varepsilon, S, d)$ , is the minimal number of balls of radius  $\varepsilon$  needed to cover the set  $S$ , i.e.,*

$$N(\varepsilon, S, d) := \min\{k : \text{There exist } y_1, \dots, y_k \in \Omega \text{ such that } S \subseteq \bigcup_{i=1}^k B_\varepsilon(y_i)\},$$

where  $B_\varepsilon(y) = \{y' \in \Omega : d(y, y') \leq \varepsilon\}$  denotes the closed  $\varepsilon$ -ball centered at  $y \in \Omega$ .

## S.2 Verification of Model Assumptions

**Proposition 3.** *The Wasserstein space  $(\Omega, d_W)$  defined in Example 1 satisfies Assumptions (L1)–(iii).*

*Proof.* As discussed in Example 1 of Chen and Müller (2022), the Wasserstein space  $(\Omega, d_W)$  satisfies the first three parts of (L1), (L2), and the first two parts of (iii) with  $\gamma_1 = \gamma_2 = 2$ . It suffices to show (L1) (iv) and (iii) (iii). For any probability distribution  $y \in \Omega$ , let  $F_y^{-1}$  be the corresponding quantile function. Let  $\langle \cdot, \cdot \rangle$ ,  $\|\cdot\|_{L^2}$ , and  $d_{L^2}(\cdot, \cdot)$  be the inner product, norm, and distance on the Hilbert space  $L^2(0, 1)$ . For any  $y \in \Omega$ , the map from  $y$  to  $F_y^{-1}$  is an isometry from  $\Omega$  to the subset of  $L^2(0, 1)$  formed by equivalence classes of left-continuous nondecreasing functions on  $(0, 1)$ . The Wasserstein space  $\Omega$  can thus be viewed as a subset of  $L^2(0, 1)$ , which has been shown to be convex and closed (Bigot et al., 2017).

Let

$$\hat{B}(\mathbf{z}) = \frac{1}{n} \sum_{i=1}^n \hat{w}(\hat{\mathbf{Z}}_i, \mathbf{z}, h) F_{Y_i}^{-1}.$$

Since

$$\begin{aligned}
\hat{Q}_h(y, \mathbf{z}) &= \frac{1}{n} \sum_{i=1}^n \hat{w}(\hat{\mathbf{Z}}_i, \mathbf{z}, h) d_{\mathcal{W}}^2(Y_i, y) \\
&= \frac{1}{n} \sum_{i=1}^n \hat{w}(\hat{\mathbf{Z}}_i, \mathbf{z}, h) [d_{L^2}^2\{F_{Y_i}^{-1}, \hat{B}(\mathbf{z})\} + d_{L^2}^2\{\hat{B}(\mathbf{z}), F_y^{-1}\} + \\
&\quad 2\langle F_{Y_i}^{-1} - \hat{B}(\mathbf{z}), \hat{B}(\mathbf{z}) - F_y^{-1} \rangle_{L^2}] \\
&= \hat{Q}_h(\hat{B}(\mathbf{z}), \mathbf{z}) + d_{L^2}^2\{\hat{B}(\mathbf{z}), F_y^{-1}\} + \\
&\quad \frac{2}{n} \sum_{i=1}^n \hat{w}(\hat{\mathbf{Z}}_i, \mathbf{z}, h) \langle F_{Y_i}^{-1} - \hat{B}(\mathbf{z}), \hat{B}(\mathbf{z}) - F_y^{-1} \rangle_{L^2}
\end{aligned}$$

and

$$\begin{aligned}
&\frac{1}{n} \sum_{i=1}^n \hat{w}(\hat{\mathbf{Z}}_i, \mathbf{z}, h) \langle F_{Y_i}^{-1} - \hat{B}(\mathbf{z}), \hat{B}(\mathbf{z}) - F_y^{-1} \rangle_{L^2} \\
&= \langle \frac{1}{n} \sum_{i=1}^n \hat{w}(\hat{\mathbf{Z}}_i, \mathbf{z}, h) F_{Y_i}^{-1} - \hat{B}(\mathbf{z}), \hat{B}(\mathbf{z}) - F_y^{-1} \rangle_{L^2} \\
&= \langle \hat{B}(\mathbf{z}) - \hat{B}(\mathbf{z}), \hat{B}(\mathbf{z}) - F_y^{-1} \rangle_{L^2} \\
&= 0,
\end{aligned}$$

One has

$$\hat{Q}_h(y, \mathbf{z}) = \hat{Q}_h(\hat{B}(\mathbf{z}), \mathbf{z}) + d_{L^2}^2\{\hat{B}(\mathbf{z}), F_y^{-1}\},$$

whence

$$\hat{v}_h(\mathbf{z}) = \arg \min_{y \in \Omega} \hat{Q}_h(y, \mathbf{z}) = \arg \min_{y \in \Omega} d_{L^2}^2\{\hat{B}(\mathbf{z}), F_y^{-1}\}.$$

Then by the convexity and closedness of the Wasserstein space, the minimizer  $\hat{v}_h(\mathbf{z})$  exists and is unique for any  $\mathbf{z} \in \mathbb{R}^r$ . Hence (L1) (iv) is satisfied.

In view of

$$\frac{1}{n} \sum_{i=1}^n \tilde{w}(\mathbf{Z}_i^0, \mathbf{z}, h) = 1,$$

one can similarly show that

$$\tilde{v}_h(\mathbf{z}) = \arg \min_{y \in \Omega} \tilde{Q}_h(y, \mathbf{z}) = \arg \min_{y \in \Omega} d_{L^2}^2\{\tilde{B}(\mathbf{z}), F_y^{-1}\},$$

where

$$\tilde{B}(\mathbf{z}) = \frac{1}{n} \sum_{i=1}^n \tilde{w}(\mathbf{Z}_i^0, \mathbf{z}, h) F_{Y_i}^{-1}.$$

Observe that  $\tilde{v}_h(\mathbf{z})$ , viewed as the best approximation of  $\tilde{B}(\mathbf{z})$  in  $\Omega$ , is characterized by

$$\langle \tilde{B}(\mathbf{z}) - F_{\tilde{v}_h(\mathbf{z})}^{-1}, F_y^{-1} - F_{\tilde{v}_h(\mathbf{z})}^{-1} \rangle_{L^2} \leq 0, \quad \text{for all } y \in \Omega.$$

It follows that

$$\begin{aligned} \tilde{Q}_h(y, \mathbf{z}) &= \frac{1}{n} \sum_{i=1}^n \tilde{w}(\mathbf{Z}_i^0, \mathbf{z}, h) d_{\mathcal{W}}^2(Y_i, y) \\ &= \tilde{Q}_h\{\tilde{v}_h(\mathbf{z}), \mathbf{z}\} + d_{\mathcal{W}}^2\{\tilde{v}_h(\mathbf{z}), y\} + \\ &\quad \frac{2}{n} \sum_{i=1}^n \tilde{w}(\mathbf{Z}_i^0, \mathbf{z}, h) \langle F_{Y_i}^{-1} - F_{\tilde{v}_h(\mathbf{z})}^{-1}, F_{\tilde{v}_h(\mathbf{z})}^{-1} - F_y^{-1} \rangle_{L^2} \\ &= \tilde{Q}_h\{\tilde{v}_h(\mathbf{z}), \mathbf{z}\} + d_{\mathcal{W}}^2\{\tilde{v}_h(\mathbf{z}), y\} + 2 \langle \tilde{B}(\mathbf{z}) - F_{\tilde{v}_h(\mathbf{z})}^{-1}, F_{\tilde{v}_h(\mathbf{z})}^{-1} - F_y^{-1} \rangle_{L^2} \\ &\geq \tilde{Q}_h\{\tilde{v}_h(\mathbf{z}), \mathbf{z}\} + d_{\mathcal{W}}^2\{\tilde{v}_h(\mathbf{z}), y\} \end{aligned}$$

for all  $y \in \Omega$ . Therefore, (iii) (iii) holds for the Wasserstein space  $(\Omega, d_{\mathcal{W}})$  for any  $\eta_3 > 0$ ,  $C_3 = 1$  and  $\gamma_3 = 2$ .

□

**Proposition 4.** *The metric space  $(\Omega, d_F)$  defined in Example 2 satisfies Assumptions (L1)–(iii), where  $\Omega$  is the space of graph Laplacians of undirected weighted networks with a fixed number of nodes  $m$  and bounded edge weights.*

*Proof.* As discussed in Theorem 3 of Zhou and Müller (2022), the space of graph Laplacians  $(\Omega, d_F)$  satisfies the first three parts of (L1), (L2), and the first two parts of (iii) with  $\gamma_1 = \gamma_2 = 2$ . It suffices to show (L1) (iv) and (iii) (iii). Let  $\langle \cdot, \cdot \rangle_F$  and  $\|\cdot\|_F$  be the Frobenius inner product and norm on  $\Omega$ . Define

$$\hat{B}(\mathbf{z}) = \frac{1}{n} \sum_{i=1}^n \hat{w}(\hat{\mathbf{Z}}_i, \mathbf{z}, h) Y_i, \quad \tilde{B}(\mathbf{z}) = \frac{1}{n} \sum_{i=1}^n \tilde{w}(\mathbf{Z}_i^0, \mathbf{z}, h) Y_i.$$

Similar to the proof of Proposition 3, one can show that

$$\hat{v}_h(\mathbf{z}) = \arg \min_{y \in \Omega} d_F^2\{\hat{B}(\mathbf{z}), y\}, \quad \tilde{v}_h(\mathbf{z}) = \arg \min_{y \in \Omega} d_F^2\{\tilde{B}(\mathbf{z}), y\}.$$

Then by the convexity and closedness of the space of graph Laplacians, the minimizer  $\hat{v}_h(\mathbf{z})$  exists and is unique for any  $\mathbf{z} \in \mathbb{R}^r$ . Hence (L1) (iv) is satisfied.

Observe that  $\tilde{v}_h(\mathbf{z})$ , viewed as the best approximation of  $\tilde{B}(\mathbf{z})$  in  $\Omega$ , is characterized by

$$\langle \tilde{B}(\mathbf{z}) - \tilde{v}_h(\mathbf{z}), y - \tilde{v}_h(\mathbf{z}) \rangle_F \leq 0, \quad \text{for all } y \in \Omega.$$

It follows that

$$\begin{aligned} \tilde{Q}_h(y, \mathbf{z}) &= \frac{1}{n} \sum_{i=1}^n \tilde{w}(\mathbf{Z}_i^0, \mathbf{z}, h) d_F^2(Y_i, y) \\ &= \tilde{Q}_h\{\tilde{v}_h(\mathbf{z}), \mathbf{z}\} + d_F^2\{\tilde{v}_h(\mathbf{z}), y\} + \\ &\quad \frac{2}{n} \sum_{i=1}^n \tilde{w}(\mathbf{Z}_i^0, \mathbf{z}, h) \langle Y_i - \tilde{v}_h(\mathbf{z}), \tilde{v}_h(\mathbf{z}) - y \rangle_F \\ &= \tilde{Q}_h\{\tilde{v}_h(\mathbf{z}), \mathbf{z}\} + d_F^2\{\tilde{v}_h(\mathbf{z}), y\} + 2\langle \tilde{B}(\mathbf{z}) - \tilde{v}_h(\mathbf{z}), \tilde{v}_h(\mathbf{z}) - y \rangle_F \\ &\geq \tilde{Q}_h\{\tilde{v}_h(\mathbf{z}), \mathbf{z}\} + d_F^2\{\tilde{v}_h(\mathbf{z}), y\} \end{aligned}$$

for all  $y \in \Omega$ . Therefore, (iii) (iii) holds for the space of graph Laplacians  $(\Omega, d_F)$  for any  $\eta_3 > 0$ ,  $C_3 = 1$  and  $\gamma_3 = 2$ .  $\square$

**Proposition 5.** *The metric space  $(\Omega, d_F)$  defined in Example 3 satisfies Assumptions (L1)–(iii), where  $\Omega$  is the space of  $m$ -dimensional covariance matrices with bounded variances or correlation matrices.*

The proof of Proposition 5 is similar to that of Proposition 4 and is thus omitted.

### S.3 Proof of Theorem 1

To establish the convergence of estimation error, Schmidt-Hieber (2020) applied an oracle-type inequality in his Theorem 2, supported by Lemma 4. In contrast to Schmidt-Hieber

(2020) where the prediction error was studied assuming independent Gaussian noise with mean 0, here we consider the case of dependent sub-Gaussian noise with possible bias that vanishes asymptotically as in (13). Additionally, we investigate both out-of-sample and in-sample errors, given that the output of deep neural networks serves as the input for local Fréchet regression. Understanding the in-sample error is crucial for examining the convergence rate of local Fréchet regression. Revisiting Lemma 4 of Schmidt-Hieber (2020), we provide here a parallel result, Lemma 2, that is suitable for the type of dependent sub-Gaussian noise with bias that we assume for our data. Theorem 1 then follows along similar arguments as in Theorem 1 and Corollary 1 of Schmidt-Hieber (2020).

**Lemma 1.** *Let  $\xi_1, \dots, \xi_M$  be sub-Gaussian random variables with mean 0 and a common parameter  $C$ , then*

$$E(\max_{l=1, \dots, M} \xi_l^2) \lesssim \log M.$$

*Proof.* By the sub-Gaussian assumption, we have  $P(|\xi_l| \geq \sqrt{t}) \leq 2e^{-t/C^2}$ . For any  $u > 0$ , we can apply the union bound and observe the following:

$$\begin{aligned} E(\max_{l=1, \dots, M} \xi_l^2) &\leq u + \int_u^\infty P(\max_{l=1, \dots, M} \xi_l^2 \geq t) dt \\ &\leq u + \sum_{l=1}^M \int_u^\infty P(|\xi_l| \geq \sqrt{t}) dt \\ &\leq u + 2M \int_u^\infty e^{-t/C^2} dt \\ &= u + 2MC^2 e^{-u/C^2}. \end{aligned}$$

By selecting  $u \asymp \log M$ , we conclude that

$$E(\max_{l=1, \dots, M} \xi_l^2) \lesssim \log M.$$

□

**Lemma 2.** Consider the  $p$ -variate nonparametric regression model (13) with unknown regression function  $g_{0j}$ . Let  $\tilde{g}_j$  be any estimator taking values in  $\mathcal{G} = \mathcal{G}(L, s, \mathbf{p}, D)$  as per (3) and  $N_\delta = N(\delta, \mathcal{G}, \|\cdot\|_\infty)$  be the covering number of  $\mathcal{G}$  using balls of size  $\delta$ . Define

$$\Delta_n = E\left[\frac{1}{n} \sum_{i=1}^n \{Z_{ij} - \tilde{g}_j(\mathbf{X}_i)\}^2 - \inf_{g \in \mathcal{G}} \frac{1}{n} \sum_{i=1}^n \{Z_{ij} - g(\mathbf{X}_i)\}^2\right]$$

and assume  $\|g_{0j}\|_\infty \leq D$ . Then for any  $i = 1, \dots, n$  and  $j = 1, \dots, r$ , we have

$$E[\{\tilde{g}_j(\mathbf{X}_i) - g_{0j}(\mathbf{X}_i)\}^2] \lesssim \inf_{g \in \mathcal{G}} E[\{g(\mathbf{X}) - g_{0j}(\mathbf{X})\}^2] + \frac{\log N_\delta}{n} + \Delta_n + \delta + |u_{nj}| \quad (22)$$

and

$$E[\{\tilde{g}_j(\mathbf{X}) - g_{0j}(\mathbf{X})\}^2] \lesssim \inf_{g \in \mathcal{G}} E[\{g(\mathbf{X}) - g_{0j}(\mathbf{X})\}^2] + \frac{\log N_\delta}{n} + \Delta_n + \delta + |u_{nj}|, \quad (23)$$

with  $\mathbf{X}$  being an independent copy of  $\mathbf{X}_1$ .

*Proof.* Define  $\|g\|_n^2 = \frac{1}{n} \sum_{k=1}^n g(\mathbf{X}_k)^2$ . Since  $E[\{\tilde{g}_j(\mathbf{X}_i) - g_{0j}(\mathbf{X}_i)\}^2] \leq 4D^2$  and  $E[\{\tilde{g}_j(\mathbf{X}) - g_{0j}(\mathbf{X})\}^2] \leq 4D^2$ , the inequality in (22) and (23) hold trivially if  $\log N_\delta \geq n$ . In the following, we focus on the case  $\log N_\delta < n$ .

Similar to Lemma 4 of Schmidt-Hieber (2020), the proof is divided into three parts which are denoted by (I)–(III).

(I) Relate the in-sample error  $E[\{\tilde{g}_j(\mathbf{X}_i) - g_{0j}(\mathbf{X}_i)\}^2]$  and predicted error  $E[\{\tilde{g}_j(\mathbf{X}) - g_{0j}(\mathbf{X})\}^2]$  to  $E(\|\tilde{g}_j - g_{0j}\|_n^2)$  via the inequality

$$E[\{\tilde{g}_j(\mathbf{X}_i) - g_{0j}(\mathbf{X}_i)\}^2] \lesssim E(\|\tilde{g}_j - g_{0j}\|_n^2) + \frac{\log N_\delta}{n} + \delta. \quad (24)$$

$$E[\{\tilde{g}_j(\mathbf{X}) - g_{0j}(\mathbf{X})\}^2] \lesssim E(\|\tilde{g}_j - g_{0j}\|_n^2) + \frac{\log N_\delta}{n} + \delta. \quad (25)$$

(II) For any estimator  $\tilde{g}_j$  taking values in  $\mathcal{G}$ ,

$$|E\{\frac{1}{n} \sum_{k=1}^n \epsilon_{kj} \pi_j(\mathbf{X}_1, \dots, \mathbf{X}_n) \tilde{g}_j(\mathbf{X}_k)\}| \lesssim \sqrt{\frac{E(\|\tilde{g}_j - g_{0j}\|_n^2) \log N_\delta}{n}} + \delta$$



(III) Show that

$$E(\|\tilde{g}_j - g_{0j}\|_n^2) \lesssim \inf_{g \in \mathcal{G}} E[\{g(\mathbf{X}) - g_{0j}(\mathbf{X})\}^2] + \frac{\log N_\delta}{n} + \Delta_n + \delta + |u_{nj}|.$$

The inequality in (22) and (23) follow from (I) and (III).

(I): Since the inequality (25) has been shown by Lemma 4(I) in Schmidt-Hieber (2020), we only need to show the inequality (24). Given a minimal  $\delta$ -covering of  $\mathcal{G}$ , denote the centers of the balls by  $g_l$ . By construction, there exists a  $l^*$  such that  $\|\tilde{g} - g_{l^*}\|_\infty \leq \delta$ . Without loss of generality, one can assume that  $\|g_l\|_\infty \leq D$  by the definition of  $\mathcal{G}$ . It follows that

$$\begin{aligned} & \left| E[\{\tilde{g}_j(\mathbf{X}_i) - g_{0j}(\mathbf{X}_i)\}^2] - E\{\|\tilde{g}_j - g_{0j}\|_n^2\} \right| \\ &= \left| E\left[\frac{1}{n} \sum_{k=1}^n \{\tilde{g}_j(\mathbf{X}_i) - g_{0j}(\mathbf{X}_i)\}^2 - \{\tilde{g}_j(\mathbf{X}_k) - g_{0j}(\mathbf{X}_k)\}^2\right] \right| \\ &= \left| \frac{1}{n} \sum_{k=1}^n E[\{\tilde{g}_j(\mathbf{X}_i) - g_{l^*}(\mathbf{X}_i)\}^2 + \{g_{l^*}(\mathbf{X}_i) - g_{0j}(\mathbf{X}_i)\}^2 \right. \\ &\quad + 2\{\tilde{g}_j(\mathbf{X}_i) - g_{l^*}(\mathbf{X}_i)\}\{g_{l^*}(\mathbf{X}_i) - g_{0j}(\mathbf{X}_i)\} - \{\tilde{g}_j(\mathbf{X}_k) - g_{l^*}(\mathbf{X}_k)\}^2 \\ &\quad \left. - \{g_{l^*}(\mathbf{X}_k) - g_{0j}(\mathbf{X}_k)\}^2 - 2\{\tilde{g}_j(\mathbf{X}_k) - g_{l^*}(\mathbf{X}_k)\}\{g_{l^*}(\mathbf{X}_k) - g_{0j}(\mathbf{X}_k)\}] \right| \\ &\lesssim E\left\{\left|\frac{1}{n} \sum_{k=1}^n f_{l^*}(\mathbf{X}_k, \mathbf{X}_i)\right|\right\} + \delta \end{aligned}$$

where  $f_{l^*}(\mathbf{X}_k, \mathbf{X}_i) = \{g_{l^*}(\mathbf{X}_i) - g_{0j}(\mathbf{X}_i)\}^2 - \{g_{l^*}(\mathbf{X}_k) - g_{0j}(\mathbf{X}_k)\}^2$ . Furthermore, define  $R_{l^*} = D\sqrt{n^{-1} \log N_\delta} \vee \sqrt{E[\{g_{l^*}(\mathbf{X}_i) - g_{0j}(\mathbf{X}_i)\}^2]}$ . Using  $\|g_{l^*} - \tilde{g}_j\|_\infty \leq \delta$  and the triangle inequality, we have  $R_{l^*} \leq D\sqrt{n^{-1} \log N_\delta} + \sqrt{E[\{\tilde{g}_j(\mathbf{X}_i) - g_{0j}(\mathbf{X}_i)\}^2]} + \delta$ . Similarly, we can define  $f_l$  and  $R_l$  in the same way with  $l^*$  being replaced by  $l$ .

Set  $U = \sqrt{E[\{\tilde{g}_j(\mathbf{X}_i) - g_{0j}(\mathbf{X}_i)\}^2]}$  and  $T = \max_{l=1, \dots, N_\delta} |\sum_{i=1}^n f_l(\mathbf{X}_k, \mathbf{X}_i)/(R_l D)|$ , we

have

$$\begin{aligned}
& \left| E[\{\tilde{g}_j(\mathbf{X}_i) - g_{0j}(\mathbf{X}_i)\}^2] - E[\|\tilde{g}_j - g_{0j}\|_n^2] \right| \\
& \lesssim E\left\{ \left| \frac{1}{n} \sum_{k=1}^n f_{l^*}(\mathbf{X}_k, \mathbf{X}_i) / (R_{l^*} D) \right| R_{l^*} \right\} + \delta \\
& \lesssim \frac{1}{n} E\{T(U + \sqrt{n^{-1} \log N_\delta} + \delta)\} + \delta \\
& \lesssim \frac{1}{n} \sqrt{E(T^2)} \sqrt{E(U^2)} + \frac{1}{n} (\sqrt{n^{-1} \log N_\delta} + \delta) E(T) + \delta,
\end{aligned}$$

where the last inequality follows from the Cauchy-Schwarz inequality. Observe that  $E[f_l(\mathbf{X}_k, \mathbf{X}_i)] = 0$ ,  $|f_l(\mathbf{X}_k, \mathbf{X}_i)| \leq 4D^2$  and

$$\begin{aligned}
\text{Var}\{f_l(\mathbf{X}_k, \mathbf{X}_i)\} &= 2\text{Var}[\{g_l(\mathbf{X}_i) - g_{0j}(\mathbf{X}_i)\}^2] \cdot \mathbf{1}_{k \neq i} \\
&\leq 2E[\{g_l(\mathbf{X}_i) - g_{0j}(\mathbf{X}_i)\}^4] \\
&\leq 8D^2 R_l^2.
\end{aligned}$$

Up to now, all the settings match Lemma 4(I) of [Schmidt-Hieber \(2020\)](#). Therefore, using the same technique, we can show that

$$E[\{\tilde{g}_j(\mathbf{X}_i) - g_{0j}(\mathbf{X}_i)\}^2] \lesssim E(\|\tilde{g}_j - g_{0j}\|_n^2) + \frac{\log N_\delta}{n} + \delta.$$

(II): For any estimator  $\tilde{g}_j$  taking values in  $\mathcal{G}$ , using Jensen's inequality and Assumption [\(D1\)](#), we have

$$\begin{aligned}
& \left| E\left\{ \sum_{k=1}^n \epsilon_{kj} \pi_j(\mathbf{X}_1, \dots, \mathbf{X}_n) \{\tilde{g}_j(\mathbf{X}_k) - g_{l^*}(\mathbf{X}_k)\} \right\} \right| \\
& \leq C_{\pi_j} \delta \sum_{k=1}^n E(|\epsilon_{kj}|) \\
& \leq n \delta C_{\pi_j} \sqrt{E(\epsilon_{1j}^2)} \\
& \leq n \delta C_{\pi_j}.
\end{aligned}$$

Since

$$\begin{aligned}
& E\{\epsilon_{kj}\pi_j(\mathbf{X}_1, \dots, \mathbf{X}_n)g_{0j}(\mathbf{X}_k)\} \\
&= E[E\{\epsilon_{kj}\pi_j(\mathbf{X}_1, \dots, \mathbf{X}_n)g_{0j}(\mathbf{X}_k)|\mathbf{X}_1, \dots, \mathbf{X}_n\}] \\
&= 0,
\end{aligned}$$

we also find

$$\begin{aligned}
& \left| E\left[\frac{1}{n} \sum_{k=1}^n \epsilon_{kj}\pi_j(\mathbf{X}_1, \dots, \mathbf{X}_n)\tilde{g}_j(\mathbf{X}_k)\right] \right| \\
&= \left| E\left[\frac{1}{n} \sum_{k=1}^n \epsilon_{kj}\pi_j(\mathbf{X}_1, \dots, \mathbf{X}_n)\{\tilde{g}_j(\mathbf{X}_k) - g_{0j}(\mathbf{X}_k)\}\right] \right| \\
&\leq \left| E\left[\frac{1}{n} \sum_{k=1}^n \epsilon_{kj}\pi_j(\mathbf{X}_1, \dots, \mathbf{X}_n)\{\tilde{g}_j(\mathbf{X}_k) - g_{l^*}(\mathbf{X}_k)\}\right] \right| \\
&+ \left| E\left[\frac{1}{n} \sum_{k=1}^n \epsilon_{kj}\pi_j(\mathbf{X}_1, \dots, \mathbf{X}_n)\{g_{l^*}(\mathbf{X}_k) - g_{0j}(\mathbf{X}_k)\}\right] \right| \\
&\leq \delta C_{\pi_j} + \left| \frac{1}{\sqrt{n}} E\left[\frac{\sum_{k=1}^n \epsilon_{kj}\pi_j(\mathbf{X}_1, \dots, \mathbf{X}_n)\{g_{l^*}(\mathbf{X}_k) - g_{0j}(\mathbf{X}_k)\}}{\sqrt{n}\|g_{l^*} - g_{0j}\|_n} \|g_{l^*} - g_{0j}\|_n\right] \right| \\
&\leq \delta C_{\pi_j} + \frac{1}{\sqrt{n}} E\{|\xi_{l^*}|(\|\tilde{g}_j - g_{0j}\|_n + \delta)\}, \tag{26}
\end{aligned}$$

with

$$\xi_l = \frac{\sum_{k=1}^n \epsilon_{kj}\pi_j(\mathbf{X}_1, \dots, \mathbf{X}_n)\{g_l(\mathbf{X}_k) - g_{0j}(\mathbf{X}_k)\}}{\sqrt{n}\|g_l - g_{0j}\|_n}.$$

Given  $\mathbf{X}_1, \dots, \mathbf{X}_n$ ,  $\xi_l$  are sub-Gaussian with common parameter  $C_{\pi_j}$ . It follows from Lemma 1 that  $E(\xi_{l^*}^2) \leq E(\max_{l=1, \dots, N_\delta} \xi_l^2) \lesssim \log N_\delta$ . Using Cauchy-Schwarz inequality,

$$E\{|\xi_{l^*}|(\|\tilde{g}_j - g_{0j}\|_n + \delta)\} \lesssim \sqrt{\log N_\delta} \{\sqrt{E(\|\tilde{g}_j - g_{0j}\|_n^2)} + \delta\}. \tag{27}$$

Together with (26) and (27), the inequality in (II) follows.

(III): For any fixed  $g \in \mathcal{G}$ , it follows from the definition of  $\Delta_n$  that

$$E\left[\frac{1}{n} \sum_{k=1}^n \{Z_{kj} - \tilde{g}_j(\mathbf{X}_k)\}^2\right] \leq E\left[\frac{1}{n} \sum_{k=1}^n \{Z_{kj} - g(\mathbf{X}_k)\}^2\right] + \Delta_n.$$

Using the inequality in (II), we have

$$\begin{aligned}
E(\|\tilde{g}_j - g_{0j}\|_n^2) &= E\left[\frac{1}{n} \sum_{k=1}^n \{\tilde{g}_j(\mathbf{X}_k) - Z_{kj} + (\epsilon_{kj} + u_{nj})\pi_j(\mathbf{X}_1, \dots, \mathbf{X}_n)\}^2\right] \\
&= E\left[\frac{1}{n} \sum_{k=1}^n \{\tilde{g}_j(\mathbf{X}_k) - Z_{kj}\}^2 + \frac{1}{n} \sum_{k=1}^n (\epsilon_{kj} + u_{nj})^2 \pi_j^2(\mathbf{X}_1, \dots, \mathbf{X}_n)\right. \\
&\quad \left. + \frac{2}{n} \sum_{k=1}^n (\epsilon_{kj} + u_{nj})\pi_j(\mathbf{X}_1, \dots, \mathbf{X}_n)\{\tilde{g}_j(\mathbf{X}_k) - Z_{kj}\}\right] \\
&\leq \Delta_n + E\left[\frac{1}{n} \sum_{k=1}^n \{g(\mathbf{X}_k) - Z_{kj}\}^2 + \frac{1}{n} \sum_{k=1}^n (\epsilon_{kj} + u_{nj})^2 \pi_j^2(\mathbf{X}_1, \dots, \mathbf{X}_n)\right] \\
&\quad + \frac{2}{n} \sum_{k=1}^n (\epsilon_{kj} + u_{nj})\pi_j(\mathbf{X}_1, \dots, \mathbf{X}_n)\{\tilde{g}_j(\mathbf{X}_k) - Z_{kj}\} \\
&\leq \Delta_n + E(\|g - g_{0j}\|_n^2) + E\left\{\frac{2}{n} \sum_{k=1}^n (\epsilon_{kj} + u_{nj})^2 \pi_j^2(\mathbf{X}_1, \dots, \mathbf{X}_n)\right\} \\
&\quad + E\left\{\frac{2}{n} \sum_{k=1}^n (\epsilon_{kj} + u_{nj})\pi_j(\mathbf{X}_1, \dots, \mathbf{X}_n)\{\tilde{g}_j(\mathbf{X}_k) - Z_{kj} - g(\mathbf{X}_k) + g_{0j}(\mathbf{X}_k)\}\right\} \\
&= \Delta_n + E[\{g(\mathbf{X}) - g_{0j}(\mathbf{X})\}^2] \\
&\quad + E\left[\frac{2}{n} \sum_{k=1}^n (\epsilon_{kj} + u_{nj})\pi_j(\mathbf{X}_1, \dots, \mathbf{X}_n)\{\tilde{g}_j(\mathbf{X}_k) - g(\mathbf{X}_k)\}\right] \\
&\lesssim \Delta_n + E[\{g(\mathbf{X}) - g_{0j}(\mathbf{X})\}^2] \\
&\quad + E\left\{\frac{1}{n} \sum_{k=1}^n \epsilon_{kj}\pi_j(\mathbf{X}_1, \dots, \mathbf{X}_n)\tilde{g}_j(\mathbf{X}_k)\right\} + |u_{nj}| \\
&\lesssim \Delta_n + E[\{g(\mathbf{X}) - g_{0j}(\mathbf{X})\}^2] \\
&\quad + \sqrt{\frac{E\{\|\tilde{g}_j - g_{0j}\|_n^2\} \log N_\delta}{n}} + \delta + |u_{nj}|.
\end{aligned}$$

Finally, applying (C.4) in [Schmidt-Hieber \(2020\)](#), the result follows.  $\square$

*Proof of Theorem 1.* Using Lemma 2 to replace Lemma 4 of [Schmidt-Hieber \(2020\)](#), the remaining proof follows the proof of Theorem 1 and Corollary 1 in [Schmidt-Hieber \(2020\)](#). Let  $\tilde{g}_j = \hat{g}_j$  be the minimizer of empirical risk (14), one has  $\Delta_n = 0$ . Then for any

$i = 1, \dots, n$  and  $j = 1, \dots, r$ , we have

$$E[\{\hat{g}_j(\mathbf{X}_i) - g_{0j}(\mathbf{X}_i)\}^2] \lesssim |u_{nj}| + \kappa_n^2 \log^3 n$$

and

$$E[\{\hat{g}_j(\mathbf{X}) - g_{0j}(\mathbf{X})\}^2] \lesssim |u_{nj}| + \kappa_n^2 \log^3 n.$$

The result follows. □

## S.4 Proof of Proposition 1

We present the elementary results of an auxiliary Lemma 3 and its proof, extending the well-known results from Fan and Gijbels (1996). The key quantities of interest are  $\mu_j = E\{K_h(\mathbf{Z}^0 - \mathbf{z})(\mathbf{Z}^0 - \mathbf{z})^{\oplus j}\}$ ,  $\tau_j(y) = E\{K_h(\mathbf{Z}^0 - \mathbf{z})(\mathbf{Z}^0 - \mathbf{z})^{\oplus j} | Y = y\}$  and the estimators  $\tilde{\mu}_j = \frac{1}{n} \sum_{i=1}^n K_h(\mathbf{Z}_i^0 - \mathbf{z})(\mathbf{Z}_i^0 - \mathbf{z})^{\oplus j}$ , for  $j = 0, 1, 2$ . These quantities are fundamental in local linear smoother, as they relate to the bias and variance properties of local Fréchet regression.

**Lemma 3.** *Suppose (K1) and (P1) hold. Then,*

$$\begin{aligned} \mu_0 &= f_{\mathbf{Z}^0}(\mathbf{z})K_{10} + O(h^2), \\ \mu_1 &= h^2 K_{12} \frac{\partial f_{\mathbf{Z}^0}(\mathbf{z})}{\partial \mathbf{z}} + O(h^3 \mathbf{1}), \\ \mu_2 &= h^2 f_{\mathbf{Z}^0}(\mathbf{z})K_{12} + O(h^4 \mathbf{1}\mathbf{1}^\top), \end{aligned}$$

where  $K_{1j} = \int_{\mathbb{R}^r} K(\mathbf{u})\mathbf{u}^{\oplus j} d\mathbf{u}$  for  $j = 0, 2$ . Furthermore, we have

$$\tilde{\mu}_j = \mu_j + O_p\{(h^{2j-r} n^{-1})^{1/2} \mathbf{1}^{\oplus j}\}$$

and

$$\begin{aligned}\tau_0(y) &= f_{\mathbf{Z}^0|Y}(\mathbf{z}, y)K_{10} + O(h^2), \\ \tau_1(y) &= h^2 K_{12} \frac{\partial f_{\mathbf{Z}^0|Y}(\mathbf{z}, y)}{\partial \mathbf{z}} + O(h^3 \mathbf{1}), \\ \tau_2(y) &= h^2 f_{\mathbf{Z}^0|Y}(\mathbf{z}, y)K_{12} + O(h^4 \mathbf{1}\mathbf{1}^\top),\end{aligned}$$

where the order term is uniform over  $y \in \Omega$ .

*Proof.* By definition, we have

$$\begin{aligned}\mu_j &= E\{K_h(\mathbf{Z}^0 - \mathbf{z})(\mathbf{Z}^0 - \mathbf{z})^{\oplus j}\} \\ &= \int h^{-r} K\{H^{-1}(\mathbf{x} - \mathbf{z})\}(\mathbf{x} - \mathbf{z})^{\oplus j} f_{\mathbf{Z}^0}(\mathbf{x}) d\mathbf{x}, \\ \tau_j(y) &= E\{K_h(\mathbf{Z}^0 - \mathbf{z})(\mathbf{Z}^0 - \mathbf{z})^{\oplus j} | Y = y\} \\ &= \int h^{-r} K\{H^{-1}(\mathbf{x} - \mathbf{z})\}(\mathbf{x} - \mathbf{z})^{\oplus j} f_{\mathbf{Z}^0|Y}(\mathbf{x}, y) d\mathbf{x}.\end{aligned}$$

The statements regarding  $\mu_j$  and  $\tau_j(y)$  follow from Assumptions (K1) and (P1) using a second-order Taylor expansion of the densities  $f_{\mathbf{Z}^0}$  and  $f_{\mathbf{Z}^0|Y}$ .

$$\begin{aligned}\mu_0 &= \int h^{-r} K\{H^{-1}(\mathbf{x} - \mathbf{z})\} f_{\mathbf{Z}^0}(\mathbf{x}) d\mathbf{x} \\ &= \int K(\mathbf{u}) f_{\mathbf{Z}^0}(\mathbf{z} + H\mathbf{u}) d\mathbf{u} \\ &= f_{\mathbf{Z}^0}(\mathbf{z})K_{10} + h\left(\frac{\partial f_{\mathbf{Z}^0}(\mathbf{z})}{\partial \mathbf{z}}\right)^\top K_{11} + O(h^2) \\ &= f_{\mathbf{Z}^0}(\mathbf{z})K_{10} + O(h^2).\end{aligned}$$

$$\begin{aligned}\mu_1 &= \int h^{-r} K\{H^{-1}(\mathbf{x} - \mathbf{z})\}(\mathbf{x} - \mathbf{z}) f_{\mathbf{Z}^0}(\mathbf{x}) d\mathbf{x} \\ &= h \int \mathbf{u} K(\mathbf{u}) f_{\mathbf{Z}^0}(\mathbf{z} + H\mathbf{u}) d\mathbf{u} \\ &= h\left\{f_{\mathbf{Z}^0}(\mathbf{z})K_{11} + hK_{12} \frac{\partial f_{\mathbf{Z}^0}(\mathbf{z})}{\partial \mathbf{z}} + O(h^2)\right\} \\ &= h^2 K_{12} \frac{\partial f_{\mathbf{Z}^0}(\mathbf{z})}{\partial \mathbf{z}} + O(h^3 \mathbf{1}).\end{aligned}$$

$$\begin{aligned}
\mu_2 &= \int h^{-r} K\{H^{-1}(\mathbf{x} - \mathbf{z})\}(\mathbf{x} - \mathbf{z})(\mathbf{x} - \mathbf{z})^\top f_{\mathbf{Z}^0}(\mathbf{x}) d\mathbf{x} \\
&= h^2 \int \mathbf{u}\mathbf{u}^\top K(\mathbf{u}) f_{\mathbf{Z}^0}(\mathbf{z} + H\mathbf{u}) d\mathbf{u} \\
&= h^2 \left\{ f_{\mathbf{Z}^0}(\mathbf{z}) K_{12} + h \int \mathbf{u}\mathbf{u}^\top \mathbf{u}^\top \frac{\partial f_{\mathbf{Z}^0}(\mathbf{z})}{\partial \mathbf{z}} K(\mathbf{u}) d\mathbf{u} + O(h^2 \mathbf{1}\mathbf{1}^\top) \right\} \\
&= h^2 f_{\mathbf{Z}^0}(\mathbf{z}) K_{12} + O(h^4 \mathbf{1}\mathbf{1}^\top).
\end{aligned}$$

$$\begin{aligned}
\tau_0(y) &= \int h^{-r} K\{H^{-1}(\mathbf{x} - \mathbf{z})\} f_{\mathbf{Z}^0|Y}(\mathbf{x}, y) d\mathbf{x} \\
&= \int K(\mathbf{u}) f_{\mathbf{Z}^0|Y}(\mathbf{z} + H\mathbf{u}, y) d\mathbf{u} \\
&= f_{\mathbf{Z}^0|Y}(\mathbf{z}, y) K_{10} + h \left( \frac{\partial f_{\mathbf{Z}^0|Y}(\mathbf{z}, y)}{\partial \mathbf{z}} \right)^\top K_{11} + O(h^2) \\
&= f_{\mathbf{Z}^0|Y}(\mathbf{z}, y) K_{10} + O(h^2).
\end{aligned}$$

$$\begin{aligned}
\tau_1(y) &= \int h^{-r} K\{H^{-1}(\mathbf{x} - \mathbf{z})\}(\mathbf{x} - \mathbf{z}) f_{\mathbf{Z}^0|Y}(\mathbf{x}, y) d\mathbf{x} \\
&= h \int \mathbf{u} K(\mathbf{u}) f_{\mathbf{Z}^0|Y}(\mathbf{z} + H\mathbf{u}, y) d\mathbf{u} \\
&= h \left\{ f_{\mathbf{Z}^0|Y}(\mathbf{z}, y) K_{11} + h K_{12} \frac{\partial f_{\mathbf{Z}^0|Y}(\mathbf{z}, y)}{\partial \mathbf{z}} + O(h^2 \mathbf{1}) \right\} \\
&= h^2 K_{12} \frac{\partial f_{\mathbf{Z}^0|Y}(\mathbf{z}, y)}{\partial \mathbf{z}} + O(h^3 \mathbf{1}).
\end{aligned}$$

$$\begin{aligned}
\tau_2(y) &= \int h^{-r} K\{H^{-1}(\mathbf{x} - \mathbf{z})\}(\mathbf{x} - \mathbf{z})(\mathbf{x} - \mathbf{z})^\top f_{\mathbf{Z}^0|Y}(\mathbf{x}, y) d\mathbf{x} \\
&= h^2 \int \mathbf{u}\mathbf{u}^\top K(\mathbf{u}) f_{\mathbf{Z}^0|Y}(\mathbf{z} + H\mathbf{u}, y) d\mathbf{u} \\
&= h^2 \left\{ f_{\mathbf{Z}^0|Y}(\mathbf{z}, y) K_{12} + h \int \mathbf{u}\mathbf{u}^\top \mathbf{u}^\top \frac{\partial f_{\mathbf{Z}^0|Y}(\mathbf{z}, y)}{\partial \mathbf{z}} K(\mathbf{u}) d\mathbf{u} + O(h^2 \mathbf{1}\mathbf{1}^\top) \right\} \\
&= h^2 f_{\mathbf{Z}^0|Y}(\mathbf{z}, y) K_{12} + O(h^4 \mathbf{1}\mathbf{1}^\top).
\end{aligned}$$

Next, by definition

$$\tilde{\mu}_j = \frac{1}{n} \sum_{i=1}^n K_h(\mathbf{Z}_i^0 - \mathbf{z})(\mathbf{Z}_i^0 - \mathbf{z})^{\oplus j}.$$

Note that  $E(\tilde{\mu}_j) = \mu_j$  and

$$E\{K_h^2(\mathbf{Z}_i^0 - \mathbf{z})(\mathbf{Z}_{il} - z_l)^{2j}\} = h^{2j-r} \int K(\mathbf{u})^2 u_l^{2j} f_{\mathbf{Z}^0}(\mathbf{z} + H\mathbf{u}) d\mathbf{u} = O(h^{2j-r}),$$

where  $Z_{il}$  is the  $l$ th element of the random vector  $\mathbf{Z}_i^0$  and  $z_l$  is the  $l$ th element of the vector  $\mathbf{z}$ . It follows that  $\text{Var}(\tilde{\mu}_j) = O(h^{2j-r}n^{-1}\mathbf{1}^{\oplus j})$ , proving the result for the  $\tilde{\mu}_j$ .  $\square$

**Lemma 4.** *Suppose (K1) and (L1) hold and furthermore  $h \rightarrow 0$ ,  $nh^r \rightarrow \infty$ . Then  $d\{\tilde{v}_h(\mathbf{z}), v_h(\mathbf{z})\} = o_p(1)$ .*

*Proof.* The symbol  $\rightsquigarrow$  denotes weak convergence and the notation  $l^\infty(\Omega)$  denotes the space of bounded functions on  $\Omega$ . According to Corollary 3.2.3 in [Van der Vaart and Wellner \(2023\)](#) and Assumption (L1) (i), it is sufficient to demonstrate the convergence of  $\sup_{y \in \Omega} |\tilde{Q}_h(y, \mathbf{z}) - Q_h(y, \mathbf{z})|$  to zero in probability. Achieving this requires showing  $Q_h(\cdot, \mathbf{z}) - \tilde{Q}_h(\cdot, \mathbf{z}) \rightsquigarrow 0$  in  $l^\infty(\Omega)$  and then applying Theorem 1.3.6 of [Van der Vaart and Wellner \(2023\)](#). Finally, by Theorem 1.5.4 and 1.5.7 in [Van der Vaart and Wellner \(2023\)](#), we can establish weak convergence by showing the following:

(i)  $\tilde{Q}_h(y, \mathbf{z}) - Q_h(y, \mathbf{z}) = o_p(1)$  for all  $y \in \Omega$  and

(ii)  $\tilde{Q}_h(\cdot, \mathbf{z}) - Q_h(\cdot, \mathbf{z})$  is asymptotically equicontinuous in probability, i.e., for all  $\epsilon, \eta > 0$ , there exists  $\delta > 0$  such that

$$\limsup_n P\left(\sup_{d(y_1, y_2) < \delta} |\{\tilde{Q}_h(y_1, \mathbf{z}) - Q_h(y_1, \mathbf{z})\} - \{\tilde{Q}_h(y_2, \mathbf{z}) - Q_h(y_2, \mathbf{z})\}| > \epsilon\right) < \eta.$$

To begin with (i), recall that

$$w(\mathbf{Z}_i^0, \mathbf{z}, h) = \frac{1}{\sigma_0^2} K_h(\mathbf{Z}_i^0 - \mathbf{z}) [1 - \mu_1^\top \mu_2^{-1}(\mathbf{Z}_i^0 - \mathbf{z})]$$

and

$$\tilde{w}(\mathbf{Z}_i^0, \mathbf{z}, h) = \frac{1}{\tilde{\sigma}_0^2} K_h(\mathbf{Z}_i^0 - \mathbf{z}) [1 - \tilde{\mu}_1^\top \tilde{\mu}_2^{-1}(\mathbf{Z}_i^0 - \mathbf{z})],$$



where  $\sigma_0^2 = \mu_0 - \mu_1^\top \mu_2^{-1} \mu_1$  and  $\tilde{\sigma}_0^2 = \tilde{\mu}_0 - \tilde{\mu}_1^\top \tilde{\mu}_2^{-1} \tilde{\mu}_1$ . Then, one observes that

$$\begin{aligned} \tilde{Q}_h(y, \mathbf{z}) - Q_h(y, \mathbf{z}) &= \frac{1}{n} \sum_{i=1}^n \{\tilde{w}(\mathbf{Z}_i^0, \mathbf{z}, h) - w(\mathbf{Z}_i^0, \mathbf{z}, h)\} d^2(Y_i, y) + \\ &\quad \frac{1}{n} \sum_{i=1}^n [w(\mathbf{Z}_i^0, \mathbf{z}, h) d^2(Y_i, y) - E\{w(\mathbf{Z}_i^0, \mathbf{z}, h) d^2(Y_i, y)\}]. \end{aligned} \quad (28)$$

Observe that  $\tilde{w}(\mathbf{Z}_i^0, \mathbf{z}, h) - w(\mathbf{Z}_i^0, \mathbf{z}, h) = W_{0n} K_h(\mathbf{Z}_i^0 - \mathbf{z}) + K_h(\mathbf{Z}_i^0 - \mathbf{z}) W_{1n}(\mathbf{Z}_i^0 - \mathbf{z})$ , where

$$W_{0n} = \frac{1}{\tilde{\sigma}_0^2} - \frac{1}{\sigma_0^2}, \quad W_{1n} = \frac{\tilde{\mu}_1^\top \tilde{\mu}_2^{-1}}{\tilde{\sigma}_0^2} - \frac{\mu_1^\top \mu_2^{-1}}{\sigma_0^2}. \quad (29)$$

Using the results of Lemma 3 and Sherman-Morrison formula, it follows that

$$\begin{aligned} &\tilde{\mu}_2^{-1} \tilde{\mu}_1 - \mu_2^{-1} \mu_1 \\ &= [\mu_2 + O_p\{(h^{4-r} n^{-1})^{1/2} \mathbf{1} \mathbf{1}^\top\}]^{-1} [\mu_1 + O_p\{(h^{2-r} n^{-1})^{1/2} \mathbf{1}\}] - \mu_2^{-1} \mu_1 \\ &= [\mu_2^{-1} - \frac{\mu_2^{-1} O_p\{(h^{4-r} n^{-1})^{1/2} \mathbf{1} \mathbf{1}^\top\} \mu_2^{-1}}{1 + \mathbf{1}^\top \mu_2^{-1} \mathbf{1}}] [\mu_1 + O_p\{(h^{2-r} n^{-1})^{1/2} \mathbf{1}\}] - \mu_2^{-1} \mu_1 \\ &= O_p\{(nh^{2+r})^{-1/2} \mathbf{1}\}. \end{aligned}$$

Furthermore, it is easy to get  $\tilde{\sigma}_0^2 - \sigma_0^2 = O_p\{(nh^r)^{-1/2}\}$ . Therefore,  $W_{0n} = O_p\{(nh^r)^{-1/2}\}$  and  $W_{1n} = O_p\{(nh^{2+r})^{-1/2} \mathbf{1}\}$ . Since for  $j = 0, 1$ , we have

$$\begin{aligned} E\{K_h(\mathbf{Z}_i^0 - \mathbf{z})(Z_{il} - z_l)^j d^2(Y_i, y)\} &= O(h^j), \\ E\{K_h^2(\mathbf{Z}_i^0 - \mathbf{z})(Z_{il} - z_l)^{2j} d^4(Y_i, y)\} &= O(h^{2j-r}), \end{aligned}$$

it follows that the first term in (28) is  $O_p((nh^r)^{-1/2})$ . We find that  $E\{w^2(\mathbf{Z}_i^0, \mathbf{z}, h)\} = O(h^{-r})$ , so the second term in (28) is  $O_p\{(nh^r)^{-1/2}\}$  as well. Then, we show that  $\tilde{Q}_h(y, \mathbf{z}) - Q_h(y, \mathbf{z}) = o_p(1)$  for any  $y \in \Omega$  and any  $\mathbf{z} \in \mathbb{R}^r$ , since  $nh^r \rightarrow \infty$ .

Moving on to (ii), for any  $y_1, y_2 \in \Omega$ ,

$$\begin{aligned}
& |\{\tilde{Q}_h(y_1, \mathbf{z}) - Q_h(y_1, \mathbf{z})\} - \{\tilde{Q}_h(y_2, \mathbf{z}) - Q_h(y_2, \mathbf{z})\}| \\
& \leq |\tilde{Q}_h(y_1, \mathbf{z}) - \tilde{Q}_h(y_2, \mathbf{z})| + |Q_h(y_1, \mathbf{z}) - Q_h(y_2, \mathbf{z})| \\
& \leq \frac{1}{n} \sum_{i=1}^n |\tilde{w}(\mathbf{Z}_i^0, \mathbf{z}, h)| |d(Y_i, y_1) - d(Y_i, y_2)| |d(Y_i, y_1) + d(Y_i, y_2)| \\
& \quad + |E[w(\mathbf{Z}_i^0, \mathbf{z}, h)\{d(Y_i, y_1) + d(Y_i, y_2)\}\{d(Y_i, y_1) - d(Y_i, y_2)\}]| \\
& \leq 2\text{diam}(\Omega)d(y_1, y_2) \frac{1}{n} \sum_{i=1}^n \{|\tilde{w}(\mathbf{Z}_i^0, \mathbf{z}, h)| + E|w(\mathbf{Z}_i^0, \mathbf{z}, h)|\} \\
& = O_p\{d(y_1, y_2)\},
\end{aligned}$$

since  $E\{|w(\mathbf{Z}_i^0, \mathbf{z}, h)|\} = O(1)$ ,  $E\{w^2(\mathbf{Z}_i^0, \mathbf{z}, h)\} = O(h^{-1})$ , and  $n^{-1} \sum_{i=1}^n |\tilde{w}(\mathbf{Z}_i^0, \mathbf{z}, h)| = O_p(1)$ . Therefore,

$$\sup_{d(y_1, y_2) < \delta} |\{\tilde{Q}_h(y_1, \mathbf{z}) - Q_h(y_1, \mathbf{z})\} - \{\tilde{Q}_h(y_2, \mathbf{z}) - Q_h(y_2, \mathbf{z})\}| = O_p(\delta),$$

which implies (ii). These show that  $d\{\tilde{v}_h(\mathbf{z}), v_h(\mathbf{z})\} = o_p(1)$ .  $\square$

*Proof of Proposition 1.* Firstly, we prove (18). Similar to the proof of Theorem 3 in [Petersen and Müller \(2019\)](#), we can show

$$\frac{dF_{Y|\mathbf{Z}^0}(\mathbf{z}, y)}{dF_Y(y)} = \frac{f_{\mathbf{Z}^0|Y}(\mathbf{z}, y)}{f_{\mathbf{Z}^0}(\mathbf{z})}$$

for all  $\mathbf{z}$  given that  $f_{\mathbf{Z}^0}(\mathbf{z}) > 0$ . Then by Lemma 3,

$$\int w(\mathbf{x}, \mathbf{z}, h) dF_{\mathbf{Z}^0|Y}(\mathbf{x}|y) = \frac{\tau_0(y) - \mu_1^\top \mu_2^{-1} \tau_1(y)}{\mu_0 - \mu_1^\top \mu_2^{-1} \mu_1} = \frac{f_{\mathbf{Z}^0|Y}(\mathbf{z}, y)}{f_{\mathbf{Z}^0}(\mathbf{z})} + O(h^2)$$

where the error term is uniform over  $y \in \Omega$ . Hence,

$$\begin{aligned}
Q_h(\omega, \mathbf{z}) &= \int d^2(y, \omega) w(\mathbf{x}, \mathbf{z}, h) dF_{\mathbf{Z}^0, Y}(\mathbf{x}, y) = \int w(\mathbf{x}, \mathbf{z}, h) dF_{\mathbf{Z}^0|Y}(\mathbf{x}, y) d^2(y, \omega) dF_Y(y) \\
&= \int \frac{f_{\mathbf{Z}^0|Y}(\mathbf{z}, y)}{f_{\mathbf{Z}^0}(\mathbf{z})} d^2(y, \omega) dF_Y(y) + O(h^2) = \int d^2(y, \omega) dF_{Y|\mathbf{Z}^0}(\mathbf{z}, y) + O(h^2) \\
&= Q(\omega, \mathbf{z}) + O(h^2),
\end{aligned}$$

where the error term is now uniform over  $\omega \in \Omega$ . By the first two parts of Assumption (L1) and employing proof by contradiction, we then have  $d\{v_h(\mathbf{z}), v(\mathbf{z})\} = o(1)$  as  $h = h_n \rightarrow 0$ .

Next, define  $r_h = h^{-\frac{\gamma_1}{\gamma_1-1}}$  and set

$$S_{j,h}(\mathbf{z}) = \{y : 2^{j-1} < r_h d\{y, v(\mathbf{z})\}^{\gamma_1/2} \leq 2^j\}.$$

Let  $I$  denote the indicator function. Then, for any  $M > 0$ , there exists  $a > 0$  such that, for large  $n$ ,

$$\begin{aligned} I[r_h d\{v_h(\mathbf{z}), v(\mathbf{z})\}^{\gamma_1/2} > 2^M] &= \sum_{j \geq M} I\{v_h(\mathbf{z}) \in S_{j,h}(\mathbf{z})\} \\ &\leq \sum_{j \geq M} I\left(\sup_{y \in S_{j,h}(\mathbf{z})} [Q_h\{v(\mathbf{z}), \mathbf{z}\} - Q_h(y, \mathbf{z})] \geq 0\right). \end{aligned}$$

By the first two parts of Assumption (iii), for every  $j$  involved in the sum, we have, for every  $y \in S_{j,h}(\mathbf{z})$ ,

$$Q\{v(\mathbf{z}), \mathbf{z}\} - Q(y, \mathbf{z}) \lesssim -d\{v(\mathbf{z}), y\}^{\gamma_1} \lesssim -\frac{2^{2(j-1)}}{r_h^2}.$$

Define  $V(y, \mathbf{z}) = Q_h(y, \mathbf{z}) - Q(y, \mathbf{z})$  and we have

$$\begin{aligned} &\sup_{y \in S_{j,h}(\mathbf{z})} |V(y, \mathbf{z}) - V\{v(\mathbf{z}), \mathbf{z}\}| \\ &\geq \sup_{y \in S_{j,h}(\mathbf{z})} [Q_h\{v(\mathbf{z}), \mathbf{z}\} - Q_h(y, \mathbf{z})] - \sup_{y \in S_{j,h}(\mathbf{z})} [Q\{v(\mathbf{z}), \mathbf{z}\} - Q(y, \mathbf{z})]. \end{aligned}$$

Hence,

$$\begin{aligned} I[r_h d\{v_h(\mathbf{z}), v(\mathbf{z})\}^{\gamma_1/2} > 2^M] &\leq \sum_{j \geq M} I\left[\sup_{y \in S_{j,h}(\mathbf{z})} |V(y, \mathbf{z}) - V\{v(\mathbf{z}), \mathbf{z}\}| \geq \frac{2^{2(j-1)}}{r_h^2}\right] \\ &\leq \sum_{j \geq M} I\left\{ah^2 \left(\frac{2^j}{r_h}\right)^{2/\gamma_1} \geq \frac{2^{2(j-1)}}{r_h^2}\right\} \\ &\leq \sum_{j \geq M} I\left\{4ah^2 \left(\frac{2^{2j/\gamma_1-2j}}{r_h^{2/\gamma_1-2}}\right) \geq 1\right\} \\ &\leq 4a \sum_{j \geq M} \frac{2^{2j(1-\gamma_1)/\gamma_1}}{r_h^{2(1-\gamma_1)/\gamma_1} h^{-2}} \leq 4a \sum_{j \geq M} \left(\frac{1}{4^{(\gamma_1-1)/\gamma_1}}\right)^j, \end{aligned}$$

which converges since  $\gamma_1 > 1$ . Thus, for some  $M > 0$ , we have

$$d\{v_h(\mathbf{z}), v(\mathbf{z})\} \leq 2^{2M/\gamma_1} h^{2/(\gamma_1-1)}$$

for large  $n$  and hence

$$d\{v_h(\mathbf{z}), v(\mathbf{z})\} = O(h^{2/(\gamma_1-1)})$$

for large  $n$ , so we showed (18).

Secondly, we prove (19). Define  $T_n(y, \mathbf{z}) = \tilde{Q}_h(y, \mathbf{z}) - Q_h(y, \mathbf{z})$ . Letting

$$D_i(y, \mathbf{z}) = d^2(Y_i, y) - d^2\{Y_i, v_h(\mathbf{z})\},$$

we have

$$\begin{aligned} |T_n(y, \mathbf{z}) - T_n\{v_h(\mathbf{z}), \mathbf{z}\}| &\leq \left| \frac{1}{n} \sum_{i=1}^n \{\tilde{w}(\mathbf{Z}_i^0, \mathbf{z}, h) - w(\mathbf{Z}_i^0, \mathbf{z}, h)\} D_i(y, \mathbf{z}) \right| \\ &\quad + \left| \frac{1}{n} \sum_{i=1}^n [w(\mathbf{Z}_i^0, \mathbf{z}, h) D_i(y, \mathbf{z}) - E\{w(\mathbf{Z}_i^0, \mathbf{z}, h) D_i(y, \mathbf{z})\}] \right|. \end{aligned} \tag{30}$$

Since  $W_{0n}$  and  $W_{1n}$  from (29) are  $O_p\{(nh^r)^{-1/2}\}$  and  $O_p\{(nh^{2+r})^{-1/2}\mathbf{1}\}$ , respectively, and using the fact that  $|D_i(y, \mathbf{z})| \leq 2\text{diam}(\Omega)d(y, v_h(\mathbf{z}))$ , the first term on the right-hand side of (30) is  $O_p[(nh^r)^{-1/2}d\{y, v_h(\mathbf{z})\}]$ , where the  $O_p$  term is independent of  $\Omega$  and  $v_h(\mathbf{z})$ .

Thus, we can define

$$B_R = \left\{ \sup_{d(y, v_h(\mathbf{z})) < \delta} \left| \frac{1}{n} \sum_{i=1}^n \{\tilde{w}(\mathbf{Z}_i^0, \mathbf{z}, h) - w(\mathbf{Z}_i^0, \mathbf{z}, h)\} D_i(y, \mathbf{z}) \right| \leq R\delta(nh^r)^{-1/2} \right\}$$

for  $R > 0$ , so that  $P(B_R^c) \rightarrow 0$ .

Next, to control the second term on the right-hand side of (30), define the functions

$g_y : \mathbb{R}^r \times \Omega \mapsto \mathbb{R}$  by

$$g_y(x, w) = \frac{1}{\sigma_0^2} K_h(\mathbf{x} - \mathbf{z}) \{1 - \mu_1^\top \mu_2^{-1}(\mathbf{x} - \mathbf{z})\} d^2(y, w),$$

and the corresponding function class

$$\mathcal{F}_{n\delta} = \{g_y - g_{v_h(\mathbf{z})} : d\{y, v_h(\mathbf{z})\} < \delta\}.$$

An envelope function for  $\mathcal{F}_{n\delta}$  is

$$F_{n\delta}(\mathbf{z}) = \frac{2\text{diam}(\Omega)\delta}{\sigma_0^2} K_h(\mathbf{z} - \mathbf{x}) |1 - \mu_1^\top \mu_2^{-1}(\mathbf{z} - \mathbf{x})|,$$

and  $E\{F_{n\delta}^2(\mathbf{Z}^0)\} = O(\delta^2 h^{-r})$ . According to Theorem 2.7.17 of [Van der Vaart and Wellner \(2023\)](#) and Assumption (L2), we know the bracketing integral of the class  $\mathcal{F}_{n\delta}$

$$J_{[]}(\epsilon, \mathcal{F}_{n\delta}, \|\cdot\|_{\mathbf{Z}^0, Y, 2}) = \int_0^\epsilon \sqrt{1 + \log N_{[]}(\{t\{E(F_{n\delta}^2)\}^{1/2}, \mathcal{F}_{n\delta}, \|\cdot\|_{\mathbf{Z}^0, Y, 2}\} dt$$

is  $O(1)$ , where  $N_{[]}(\{t\{E(F_{n\delta}^2)\}^{1/2}, \mathcal{F}_{n\delta}, \|\cdot\|_{\mathbf{Z}^0, Y, 2}\})$  denotes the minimum number of  $t\{E(F_{n\delta}^2)\}^{1/2}$ -brackets needed to cover the function class  $\mathcal{F}_{n\delta}$  (see Definition 2.1.6 of [Van der Vaart and Wellner \(2023\)](#)) and  $\|\cdot\|_{\mathbf{Z}^0, Y, 2}$  denotes the norm that for any  $f \in \mathcal{F}_{n\delta}$ ,  $\|f\|_{\mathbf{Z}^0, Y, 2} = [E\{f(\mathbf{Z}^0, Y)^2\}]^{1/2}$ . Using these facts together with Theorems 2.14.16 of [Van der Vaart and Wellner \(2023\)](#) and Assumption (L2), for small  $\delta$ ,

$$\begin{aligned} & E \left( \sup_{d\{y, v_h(\mathbf{z})\} < \delta} \left| \frac{1}{n} \sum_{i=1}^n w(\mathbf{Z}_i^0, \mathbf{z}, h) D_i(y, \mathbf{z}) - E\{w(\mathbf{Z}_i^0, \mathbf{z}, h) D_i(y, \mathbf{z})\} \right| \right) \\ & \leq \frac{J_{[]}(\epsilon, \mathcal{F}_{n\delta}, \|\cdot\|_{\mathbf{Z}^0, Y, 2}) [E\{F_{n\delta}^2(\mathbf{Z}^0)\}]^{1/2}}{\sqrt{n}} \\ & = O(\delta(nh^r)^{-1/2}). \end{aligned}$$

Combining this with (30) and the definition of  $B_R$ ,

$$E \left( I_{B_R} \sup_{d\{y, v_h(\mathbf{z})\} < \delta} |T_n(y, \mathbf{z}) - T_n\{v_h(\mathbf{z}), \mathbf{z}\}| \right) \leq \frac{a\delta}{(nh^r)^{1/2}}, \quad (31)$$

where  $I_{B_R}$  is the indicator function for the set  $B_R$  and  $a$  is a constant depending on  $R$  and the entropy integral in Assumption (L2).

To finish, set  $r_n = (nh^r)^{\frac{\gamma_2}{4(\gamma_2-1)}}$  and define

$$S_{j,n}(\mathbf{z}) = \{y : 2^{j-1} < r_n d\{y, v_h(\mathbf{z})\}^{\gamma_2/2} \leq 2^j\}.$$

Choose  $\eta_2$  satisfying Assumption (iii) (ii) and such that Assumption (L2) is satisfied for any  $\delta < \eta_2$ . Set  $\eta = (\eta_2/2)^{\gamma_2/2}$ . Denote events  $A_{\eta_2} = \{d\{\tilde{v}_h(\mathbf{z}), v_h(\mathbf{z})\} > \eta_2/2\}$  and  $C_M = \{r_n d\{\tilde{v}_h(\mathbf{z}), v_h(\mathbf{z})\}^{\gamma_2/2} > 2^M\}$ . If  $r_n d\{\tilde{v}_h(\mathbf{z}), v_h(\mathbf{z})\}^{\gamma_2/2}$  is larger than  $2^M$  for a given integer  $M$ , then  $\tilde{v}_h(\mathbf{z})$  is in one of the shells  $S_{j,n}(\mathbf{z})$  with  $j > M$  such that the supremum of the map  $y \mapsto \tilde{Q}_h\{v_h(\mathbf{z}), \mathbf{z}\} - \tilde{Q}_h(y, \mathbf{z})$  over this shell is nonnegative by the property of  $\tilde{v}_h(\mathbf{z})$ .

$$\begin{aligned} P(C_M) &\leq P(B_R^c) + P(A_{\eta_2}) + P(B_R \cap A_{\eta_2}^c \cap C_M) \\ &\leq P(B_R^c) + P(A_{\eta_2}) + \sum_{\substack{j \geq M \\ 2^j \leq r_n \eta}} P \left( \left\{ \sup_{y \in S_{j,n}(\mathbf{z})} \left| \tilde{Q}_h\{v_h(\mathbf{z}), \mathbf{z}\} - \tilde{Q}_h(y, \mathbf{z}) \right| \geq 0 \right\} \cap B_R \right), \end{aligned}$$

where the first term goes to zero clearly and the second term goes to zero by Lemma 4. Choose  $\eta_2 > 0$  small enough that Assumption (iii) (ii) holds for every  $d\{y, v_h(\mathbf{z})\} \leq \eta$  and (31) holds for every  $\delta \leq \eta$ . Then for every  $j$  involved in the sum, we have, for every  $y \in S_{j,n}(\mathbf{z})$ ,

$$Q_h(v_h(\mathbf{z}), \mathbf{z}) - Q_h(y, \mathbf{z}) \lesssim -d\{v_h(\mathbf{z}), y\}^{\gamma_2} \lesssim -\frac{2^{2(j-1)}}{r_n^2}.$$

In terms of  $T_n(y, \mathbf{z}) = \tilde{Q}_h(y, \mathbf{z}) - Q_h(y, \mathbf{z})$ , by Markov's inequality, we have

$$\begin{aligned} P(C_M) &\leq P(B_R^c) + P(A_{\eta_2}) \\ &\quad + \sum_{\substack{j \geq M \\ 2^j \leq r_n \eta}} P \left( \left\{ \sup_{y \in S_{j,n}} |T_n(y, \mathbf{z}) - T_n\{v_h(\mathbf{z}), \mathbf{z}\}| \gtrsim \frac{2^{2(j-1)}}{r_n^2} \right\} \cap B_R \right) \\ &\lesssim \sum_{\substack{j \geq M \\ 2^j \leq r_n \eta}} \frac{(2^j/r_n)^{2/\gamma_2} (nh^r)^{-1/2}}{2^{2j}/r_n^2} \\ &\lesssim \sum_{j \geq M} \frac{2^{2j(1-\gamma_2)/\gamma_2}}{r_n^{2(1-\gamma_2)/\gamma_2} \sqrt{nh^r}} \\ &= \sum_{j \geq M} \left( \frac{1}{4^{(\gamma_2-1)/\gamma_2}} \right)^j, \end{aligned}$$

which converges since  $\gamma_2 > 1$ . Hence, as  $M \rightarrow \infty$ ,

$$P(d\{\tilde{v}_h(\mathbf{z}), v_h(\mathbf{z})\} > (\frac{2^M}{r_n})^{2/\gamma_2}) \rightarrow 0.$$

Therefore,

$$d\{\tilde{v}_h(\mathbf{z}), v_h(\mathbf{z})\} = O_p\{(nh^r)^{-1/\{2(\gamma_2-1)\}}\}.$$

□

## S.5 Proof of Proposition 2

**Lemma 5.** *Suppose (K1) holds. If  $\|\hat{\mathbf{Z}}_i - \mathbf{Z}_i^0\| = O_p(\zeta_n)$  for  $i = 1, \dots, n$ ,  $\|\hat{\mathbf{Z}} - \mathbf{Z}^0\| = O_p(\zeta_n)$ ,  $nh^r \rightarrow \infty$ , and  $h^{-r-2}\zeta_n \rightarrow 0$ , then the weight functions as defined in (10) and (16) satisfy*

$$\frac{1}{n} \sum_{i=1}^n \{\hat{w}(\hat{\mathbf{Z}}_i, \hat{\mathbf{Z}}, h) - \tilde{w}(\mathbf{Z}_i^0, \mathbf{Z}^0, h)\} = O_p(h^{-r-1}\zeta_n).$$

*Proof.* Recall that

$$\hat{w}(\hat{\mathbf{Z}}_i, \hat{\mathbf{Z}}, h) = \frac{1}{\hat{\sigma}^2} K_h(\hat{\mathbf{Z}}_i - \hat{\mathbf{Z}}) [1 - \hat{\mu}_1^T \hat{\mu}_2^{-1} (\hat{\mathbf{Z}}_i - \hat{\mathbf{Z}})],$$

where

$$\hat{\sigma}^2 = \hat{\mu}_0 - \hat{\mu}_1^T \hat{\mu}_2^{-1} \hat{\mu}_1, \quad \hat{\mu}_j = \frac{1}{n} \sum_{i=1}^n K_h(\hat{\mathbf{Z}}_i - \hat{\mathbf{Z}}) (\hat{\mathbf{Z}}_i - \hat{\mathbf{Z}})^{\oplus j}, \quad j = 0, 1, 2$$

and

$$\tilde{w}(\mathbf{Z}_i^0, \mathbf{Z}^0, h) = \frac{1}{\tilde{\sigma}^2} K_h(\mathbf{Z}_i^0 - \mathbf{Z}^0) [1 - \tilde{\mu}_1^T \tilde{\mu}_2^{-1} (\mathbf{Z}_i^0 - \mathbf{Z}^0)],$$

where

$$\tilde{\sigma}^2 = \tilde{\mu}_0 - \tilde{\mu}_1^T \tilde{\mu}_2^{-1} \tilde{\mu}_1, \quad \tilde{\mu}_j = \frac{1}{n} \sum_{i=1}^n K_h(\mathbf{Z}_i^0 - \mathbf{Z}^0) (\mathbf{Z}_i^0 - \mathbf{Z}^0)^{\oplus j}, \quad j = 0, 1, 2$$

with  $K_h(\mathbf{z}) = h^{-r} K\{H^{-1}\mathbf{z}\}$ .

Define

$$\rho_j(\mathbf{x}, \mathbf{z}) = K_h(\mathbf{x} - \mathbf{z}) (\mathbf{x} - \mathbf{z})^{\oplus j}, \quad \mathbf{x}, \mathbf{z} \in \mathcal{T}^r.$$

By Assumption (K1),  $K(\cdot)$  is Lipschitz continuous. For any  $\mathbf{x}_1, \mathbf{x}_2, \mathbf{z}_1, \mathbf{z}_2 \in \mathcal{T}^r$ , one has

$$\begin{aligned} |\rho_0(\mathbf{x}_1, \mathbf{z}_1) - \rho_0(\mathbf{x}_2, \mathbf{z}_2)| &= |K_h(\mathbf{x}_1 - \mathbf{z}_1) - K_h(\mathbf{x}_2 - \mathbf{z}_2)| \\ &\lesssim h^{-r-1} \|\mathbf{x}_1 - \mathbf{z}_1 - (\mathbf{x}_2 - \mathbf{z}_2)\| \\ &\leq h^{-r-1} (\|\mathbf{x}_1 - \mathbf{x}_2\| + \|\mathbf{z}_1 - \mathbf{z}_2\|). \end{aligned}$$

For  $j = 1, 2$ , it hold that

$$\begin{aligned} \|\rho_j(\mathbf{x}_1, \mathbf{z}_1) - \rho_j(\mathbf{x}_2, \mathbf{z}_2)\| &= \|K_h(\mathbf{x}_1 - \mathbf{z}_1)(\mathbf{x}_1 - \mathbf{z}_1)^{\oplus j} - K_h(\mathbf{x}_2 - \mathbf{z}_2)(\mathbf{x}_2 - \mathbf{z}_2)^{\oplus j}\| \\ &\leq \|K_h(\mathbf{x}_1 - \mathbf{z}_1)(\mathbf{x}_1 - \mathbf{z}_1)^{\oplus j} - K_h(\mathbf{x}_2 - \mathbf{z}_2)(\mathbf{x}_1 - \mathbf{z}_1)^{\oplus j}\| + \\ &\quad \|K_h(\mathbf{x}_2 - \mathbf{z}_2)(\mathbf{x}_1 - \mathbf{z}_1)^{\oplus j} - K_h(\mathbf{x}_2 - \mathbf{z}_2)(\mathbf{x}_2 - \mathbf{z}_2)^{\oplus j}\| \\ &\leq \|(\mathbf{x}_1 - \mathbf{z}_1)^{\oplus j}\| \cdot |K_h(\mathbf{x}_1 - \mathbf{z}_1) - K_h(\mathbf{x}_2 - \mathbf{z}_2)| + \\ &\quad K_h(\mathbf{x}_2 - \mathbf{z}_2) \cdot \|(\mathbf{x}_1 - \mathbf{z}_1)^{\oplus j} - (\mathbf{x}_2 - \mathbf{z}_2)^{\oplus j}\|. \end{aligned}$$

Using the Lipschitz continuity of  $K(\cdot)$  by Assumption (K1) and the fact that  $K_h(\mathbf{x} - \mathbf{z}) = 0$  if any component of  $|\mathbf{x} - \mathbf{z}|$  exceeds  $h$ , for  $j = 1, 2$  one has

$$\begin{aligned} \|\rho_j(\mathbf{x}_1, \mathbf{z}_1) - \rho_j(\mathbf{x}_2, \mathbf{z}_2)\| &\lesssim h^{j-r-1} \|\mathbf{x}_1 - \mathbf{z}_1 - (\mathbf{x}_2 - \mathbf{z}_2)\| + \\ &\quad h^{j-1} \|\mathbf{x}_1 - \mathbf{z}_1 - (\mathbf{x}_2 - \mathbf{z}_2)\| \\ &\lesssim h^{-r-1+j} \|\mathbf{x}_1 - \mathbf{z}_1 - (\mathbf{x}_2 - \mathbf{z}_2)\| \\ &\leq h^{-r-1+j} (\|\mathbf{x}_1 - \mathbf{x}_2\| + \|\mathbf{z}_1 - \mathbf{z}_2\|). \end{aligned}$$

One thus has

$$\begin{aligned} \|\hat{\mu}_j - \tilde{\mu}_j\| &= \left\| \frac{1}{n} \sum_{i=1}^n \rho_j(\hat{\mathbf{Z}}_i, \hat{\mathbf{Z}}) - \frac{1}{n} \sum_{i=1}^n \rho_j(\mathbf{Z}_i^0, \mathbf{Z}^0) \right\| \\ &\leq \frac{1}{n} \sum_{i=1}^n \|\rho_j(\hat{\mathbf{Z}}_i, \hat{\mathbf{Z}}) - \rho_j(\mathbf{Z}_i^0, \mathbf{Z}^0)\| \\ &\lesssim \frac{1}{n} \sum_{i=1}^n h^{-r-1+j} (\|\hat{\mathbf{Z}}_i - \mathbf{Z}_i^0\| + \|\hat{\mathbf{Z}} - \mathbf{Z}^0\|). \end{aligned}$$



We conclude that  $\|\hat{\mu}_j - \tilde{\mu}_j\| = O_p(h^{-r-1+j}\zeta_n)$  for  $j = 0, 1, 2$ . Since  $nh^r \rightarrow \infty$ , by Lemma 3 one has  $\tilde{\mu}_0 = O_p(1)$ ,  $\tilde{\mu}_1 = O_p(h^2)$ , and  $\tilde{\mu}_2 = O_p(h^2)$ . It follows that

$$\begin{aligned} |\hat{\sigma}^2 - \tilde{\sigma}^2| &= |(\hat{\mu}_0 - \hat{\mu}_1^T \hat{\mu}_2^{-1} \hat{\mu}_1) - (\tilde{\mu}_0 - \tilde{\mu}_1^T \tilde{\mu}_2^{-1} \tilde{\mu}_1)| \\ &= O_p(h^{-r-1}\zeta_n) \end{aligned}$$

and

$$\left\| \frac{\hat{\mu}_1^T \hat{\mu}_2^{-1}}{\hat{\sigma}^2} - \frac{\tilde{\mu}_1^T \tilde{\mu}_2^{-1}}{\tilde{\sigma}^2} \right\| = O_p(h^{-r-2}\zeta_n),$$

Observe that

$$\begin{aligned} \hat{w}(\hat{\mathbf{Z}}_i, \hat{\mathbf{Z}}, h) - \tilde{w}(\mathbf{Z}_i^0, \mathbf{Z}^0, h) &= \{\hat{\sigma}^{-2} - \tilde{\sigma}^{-2}\} \rho_0(\mathbf{Z}_i^0, \mathbf{Z}^0) + \hat{\sigma}^{-2} \{\rho_0(\hat{\mathbf{Z}}_i, \hat{\mathbf{Z}}) - \rho_0(\mathbf{Z}_i^0, \mathbf{Z}^0)\} - \\ &\quad \left\{ \frac{\hat{\mu}_1^T \hat{\mu}_2^{-1}}{\hat{\sigma}^2} - \frac{\tilde{\mu}_1^T \tilde{\mu}_2^{-1}}{\tilde{\sigma}^2} \right\} \rho_1(\mathbf{Z}_i^0, \mathbf{Z}^0) - \\ &\quad \frac{\hat{\mu}_1^T \hat{\mu}_2^{-1}}{\hat{\sigma}^2} \{\rho_1(\hat{\mathbf{Z}}_i, \hat{\mathbf{Z}}) - \rho_1(\mathbf{Z}_i^0, \mathbf{Z}^0)\} \end{aligned}$$

and  $E\{\rho_j(\mathbf{Z}_i^0, \mathbf{Z}^0)\} = O(h^j \mathbf{1}^{\oplus j})$ ,  $E[\{\rho_j(\mathbf{Z}_i^0, \mathbf{Z}^0)\}^{\oplus 2}] = O(h^{2j-r} \mathbf{1}^{\oplus 2j})$  for  $j = 0, 1$ . We have

$$\frac{1}{n} \sum_{i=1}^n \{\hat{w}(\hat{\mathbf{Z}}_i, \hat{\mathbf{Z}}, h) - \tilde{w}(\mathbf{Z}_i^0, \mathbf{Z}^0, h)\} = O_p(h^{-r-1}\zeta_n).$$

□

**Lemma 6.** Suppose (K1) and the last two parts of (L1). If  $\|\hat{\mathbf{Z}}_i - \mathbf{Z}_i^0\| = O_p(\zeta_n)$  for  $i = 1, \dots, n$ ,  $\|\hat{\mathbf{Z}} - \mathbf{Z}^0\| = O_p(\zeta_n)$ ,  $nh^r \rightarrow \infty$ , and  $h^{-r-2}\zeta_n \rightarrow 0$ , then the following holds,

$$d\{\hat{v}_h(\hat{\mathbf{Z}}), \tilde{v}_h(\mathbf{Z}^0)\} = o_p(1).$$

*Proof.* For any  $y \in \Omega$ , observe that

$$\begin{aligned} \hat{Q}_h(y, \hat{\mathbf{Z}}) - \tilde{Q}_h(y, \mathbf{Z}^0) &= \frac{1}{n} \sum_{i=1}^n \hat{w}(\hat{\mathbf{Z}}_i, \hat{\mathbf{Z}}, h) d^2(Y_i, y) - \frac{1}{n} \sum_{i=1}^n \tilde{w}(\mathbf{Z}_i^0, \mathbf{Z}^0, h) d^2(Y_i, y) \\ &= \frac{1}{n} \sum_{i=1}^n \{\hat{w}(\hat{\mathbf{Z}}_i, \hat{\mathbf{Z}}, h) - \tilde{w}(\mathbf{Z}_i^0, \mathbf{Z}^0, h)\} d^2(Y_i, y) \\ &= O_p(h^{-r-1}\zeta_n) \end{aligned}$$

by Lemma 5 and the fact that  $\Omega$  is totally bounded. By the last two parts of Assumption (L1) and employing proof by contradiction, one concludes that  $d\{\hat{v}_h(\hat{\mathbf{Z}}), \tilde{v}_h(\mathbf{Z}^0)\} = o_p(1)$ .

□

*Proof of Proposition 2.* Define  $V_n(y) = \hat{Q}_h(y, \hat{\mathbf{Z}}) - \tilde{Q}_h(y, \mathbf{Z}^0)$ . Letting  $D_i(y, \mathbf{Z}^0) = d^2(Y_i, y) - d^2\{Y_i, \tilde{v}_h(\mathbf{Z}^0)\}$ , we have

$$|V_n(y) - V_n\{\tilde{v}_h(\mathbf{Z}^0)\}| = \left| \frac{1}{n} \sum_{i=1}^n \{\hat{w}(\hat{\mathbf{Z}}_i, \hat{\mathbf{Z}}, h) - \tilde{w}(\mathbf{Z}_i^0, \mathbf{Z}^0, h)\} D_i(y, \mathbf{Z}^0) \right|. \quad (32)$$

By Lemma 5, and using the fact that  $|D_i(y, \mathbf{Z}^0)| \leq 2\text{diam}(\Omega)d\{y, \tilde{v}_h(\mathbf{Z}^0)\}$ , the right-hand side of (32) is  $O_p[d\{y, \tilde{v}_h(\mathbf{Z}^0)\}h^{-r-1}\zeta_n]$ . Thus, we can define

$$B_R = \left\{ \sup_{d\{y, \tilde{v}_h(\mathbf{Z}^0)\} < \delta} |V_n(y) - V_n\{\tilde{v}_h(\mathbf{Z}^0)\}| \leq R\delta h^{-r-1}\zeta_n \right\}$$

for  $R > 0$ , so that  $P(B_R^C) \rightarrow 0$ .

Set  $t_n = (h^{-r-1}\zeta_n)^{-\gamma_3/2(\gamma_3-1)}$ . For each  $n$ , the metric space  $\Omega$  (minus the point  $\tilde{v}_h(\mathbf{Z}^0)$ ) can be partitioned into the “shells”

$$S_{j,n}(\mathbf{Z}^0) = \{y : 2^{j-1} < t_n d\{y, \tilde{v}_h(\mathbf{Z}^0)\}^{\gamma_3/2} \leq 2^j\},$$

with  $j$  varying over the integers. Choose  $\eta = (\eta_3/2)^{\gamma_3/2} > 0$  small enough that Assumption (iii) (iii) holds and  $\delta < \eta_3$ . If  $t_n d\{\hat{v}_h(\hat{\mathbf{Z}}), \tilde{v}_h(\mathbf{Z}^0)\}^{\gamma_3/2}$  is larger than  $2^M$  for a given integer  $M$ , then  $\hat{v}_h(\hat{\mathbf{Z}})$  is in one of the shells  $S_{j,n}(\mathbf{Z}^0)$  with  $j > M$ . In that case the supremum of the map  $y \mapsto \hat{Q}_h(\tilde{v}_h(\mathbf{Z}^0), \hat{\mathbf{Z}}) - \hat{Q}_h(y, \hat{\mathbf{Z}})$  over this shell is nonnegative by the optimality of  $\hat{v}_h(\hat{\mathbf{Z}})$ . Conclude that, for every  $\eta > 0$ ,

$$\begin{aligned} & P(t_n d\{\hat{v}_h(\hat{\mathbf{Z}}), \tilde{v}_h(\mathbf{Z}^0)\}^{\gamma_3/2} > 2^M) \\ & \leq P(B_R^C) + P(2d\{\hat{v}_h(\hat{\mathbf{Z}}), \tilde{v}_h(\mathbf{Z}^0)\} > \eta_3) \\ & \quad + \sum_{\substack{j > M \\ 2^j \leq \eta t_n}} P(\{ \sup_{y \in S_{j,n}(\mathbf{Z}^0)} [\hat{Q}_h\{\tilde{v}_h(\mathbf{Z}^0), \hat{\mathbf{Z}}\} - \hat{Q}_h(y, \hat{\mathbf{Z}})] \geq 0\} \cap B_R), \end{aligned} \quad (33)$$

where  $P(B_R^C) \rightarrow 0$  as discussed previously and the second term goes to zero by Lemma 6. Then for every  $j$  involved in the sum, by Assumption (iii) (iii) we have, for every  $y \in S_{j,n}(\mathbf{Z}^0)$ ,

$$\tilde{Q}_h\{\tilde{v}_h(\mathbf{Z}^0), \mathbf{Z}^0\} - \tilde{Q}_h(y, \mathbf{Z}^0) \lesssim -\frac{2^{2(j-1)}}{t_n^2}.$$

In terms of the centered process  $V_n$ , by Markov's inequality the right-hand side of (33) may be bounded by

$$\begin{aligned} & \sum_{\substack{j>M \\ 2^j \leq \eta t_n}} P\left(\left\{ \sup_{y \in S_{j,n}(\mathbf{Z}^0)} [V_n(y) - V_n\{\tilde{v}_h(\mathbf{Z}^0)\}] \gtrsim \frac{2^{2(j-1)}}{t_n^2} \right\} \cap B_R\right) \\ & \lesssim \sum_{j>M} \frac{t_n^2}{2^{2j}} \left(\frac{2^j}{t_n}\right)^{2/\gamma_3} h^{-r-1} \zeta_n \\ & = \sum_{j>M} \left(\frac{1}{4^{(\gamma_3-1)/\gamma_3}}\right)^j, \end{aligned}$$

which converges to zero for every  $M = M_n \rightarrow \infty$  since  $\gamma_3 > 1$ . Hence

$$d\{\hat{v}_h(\hat{\mathbf{Z}}), \tilde{v}_h(\mathbf{Z}^0)\} = O_p(t_n^{-2/\gamma_3}) = O_p\{(h^{-r-1}\zeta_n)^{1/(\gamma_3-1)}\}.$$

□

## S.6 Proof of Theorem 2

*Proof of Theorem 2.* Combining Theorems, 1 and Proposition 1, and 2, it follows from the triangle inequality that

$$\begin{aligned} d\{\hat{m}(\mathbf{X}), m(\mathbf{X})\} &= d\{\hat{v}_h(\hat{\mathbf{Z}}), v(\mathbf{Z}^0)\} \\ &\leq d\{\tilde{v}_h(\mathbf{Z}^0), v(\mathbf{Z}^0)\} + d\{\hat{v}_h(\hat{\mathbf{Z}}), \tilde{v}_h(\mathbf{Z}^0)\} \\ &= O_p\{h^{2/(\gamma_1-1)} + (nh^r)^{-1/\{2(\gamma_2-1)\}} + (h^{-r-1}\zeta_n)^{1/(\gamma_3-1)}\}, \end{aligned}$$

where  $\mathbf{Z}^0 = \mathbf{g}_0(\mathbf{X})$  and  $\hat{\mathbf{Z}} = \hat{\mathbf{g}}(\mathbf{X})$ .

□

## S.7 Additional Proof

If we have the supremum rate,  $E(\sup_{i=1,\dots,n} \|\hat{\mathbf{Z}}_i - \mathbf{Z}_i^0\|) = O(\tau_n)$ , we can substitute Lemma 5 with Lemma 7 below. This substitution would lead to an improvement in the convergence rate outlined in Proposition 2, resulting in  $(h^{-1}\tau_n)^{1/(\gamma_3-1)}$ . Furthermore, an enhanced convergence rate can be achieved in Theorem 2, expressed as  $h^{2/(\gamma_1-1)} + (nh^r)^{-1/2(\gamma_2-1)} + (h^{-1}\tau_n)^{1/(\gamma_3-1)}$ .

**Lemma 7.** *Suppose (K1) and (P1) hold. If  $E(\sup_{i=1,\dots,n} \|\hat{\mathbf{Z}}_i - \mathbf{Z}_i^0\|) = O(\tau_n)$ ,  $nh^r \rightarrow \infty$  and  $h^{-r-1}\tau_n \rightarrow 0$ , then the weight functions as defined in (10) and (16) satisfy*

$$\frac{1}{n} \sum_{i=1}^n \{\hat{w}(\hat{\mathbf{Z}}_i, \hat{\mathbf{Z}}, h) - \tilde{w}(\mathbf{Z}_i^0, \mathbf{Z}^0, h)\} = O_p(h^{-1}\tau_n).$$

*Proof.* Recall that in Lemma 5, for any  $\mathbf{x}_1, \mathbf{x}_2, \mathbf{z}_1, \mathbf{z}_2 \in \mathcal{T}^r$ , one has

$$\|\rho_j(\mathbf{x}_1, \mathbf{z}_1) - \rho_j(\mathbf{x}_2, \mathbf{z}_2)\| \lesssim h^{-r-1+j}(\|\mathbf{x}_1 - \mathbf{x}_2\| + \|\mathbf{z}_1 - \mathbf{z}_2\|).$$

One thus has

$$\begin{aligned} \|\hat{\mu}_j - \tilde{\mu}_j\| &= \left\| \frac{1}{n} \sum_{i=1}^n \rho_j(\hat{\mathbf{Z}}_i, \hat{\mathbf{Z}}) - \frac{1}{n} \sum_{i=1}^n \rho_j(\mathbf{Z}_i^0, \mathbf{Z}^0) \right\| \\ &\leq \frac{1}{n} \sum_{i=1}^n \|\rho_j(\hat{\mathbf{Z}}_i, \hat{\mathbf{Z}}) - \rho_j(\mathbf{Z}_i^0, \mathbf{Z}^0)\| \cdot [\mathbf{I}\{\rho_j(\hat{\mathbf{Z}}_i, \hat{\mathbf{Z}}) \neq 0\} + \mathbf{I}\{\rho_j(\mathbf{Z}_i^0, \mathbf{Z}^0) \neq 0\}] \\ &\leq \frac{1}{nh^{r+1-j}} \left( \sup_{i=1,\dots,n} \|\hat{\mathbf{Z}}_i - \mathbf{Z}_i^0\| + \|\hat{\mathbf{Z}} - \mathbf{Z}^0\| \right) \\ &\quad \sum_{i=1}^n [\mathbf{I}(\|\hat{\mathbf{Z}}_i - \hat{\mathbf{Z}}\| \leq h) + \mathbf{I}(\|\mathbf{Z}_i^0 - \mathbf{Z}^0\| \leq h)] \\ &\lesssim \frac{\tau_n}{nh^{r+1-j}} \sum_{i=1}^n [\mathbf{I}(\|\hat{\mathbf{Z}}_i - \hat{\mathbf{Z}}\| \leq h) + \mathbf{I}(\|\mathbf{Z}_i^0 - \mathbf{Z}^0\| \leq h)]. \end{aligned}$$

Given  $\mathbf{Z}^0$ , observe

$$\frac{1}{nh^r} \sum_{i=1}^n \mathbf{I}(\|\mathbf{Z}_i^0 - \mathbf{Z}^0\| \leq h) \xrightarrow{P} c_1 f_{\mathbf{Z}^0}(\mathbf{Z}^0)$$

for some constant  $c_1 < \infty$ , and that

$$\begin{aligned} & \frac{1}{nh^r} \sum_{i=1}^n \mathbf{I}(\|\hat{\mathbf{Z}}_i - \hat{\mathbf{Z}}\| \leq h) \\ & \leq \frac{1}{nh^r} \sum_{i=1}^n \mathbf{I}(\|\mathbf{Z}_i^0 - \mathbf{Z}^0\| \leq 3h) + \mathbf{I}(\|\hat{\mathbf{Z}}_i - \mathbf{Z}_i^0\| \geq h) + \mathbf{I}(\|\hat{\mathbf{Z}} - \mathbf{Z}^0\| \geq h) \end{aligned}$$

converges to  $c_2 f(\mathbf{Z}_i^0)$  in probability for some constant  $c_2 < \infty$ . Here,

$$\frac{1}{nh^r} \sum_{i=1}^n \mathbf{I}(\|\hat{\mathbf{Z}}_i - \mathbf{Z}_i^0\| \geq h) \text{ and } \frac{1}{nh^r} \sum_{i=1}^n \mathbf{I}(\|\hat{\mathbf{Z}} - \mathbf{Z}^0\| \geq h)$$

are both  $o_p(1)$  since by the Markov inequality and Theorem 1,

$$\begin{aligned} E\left\{\frac{1}{nh^r} \sum_{i=1}^n \mathbf{I}(\|\hat{\mathbf{Z}}_i - \mathbf{Z}_i^0\| \geq h)\right\} & \leq \frac{1}{nh^{r+1}} \sum_{i=1}^n E\|\hat{\mathbf{Z}}_i - \mathbf{Z}_i^0\| \leq \frac{1}{n} \sum_{i=1}^n h^{-r-1} \tau_n \rightarrow 0, \\ E\left\{\frac{1}{nh^r} \sum_{i=1}^n \mathbf{I}(\|\hat{\mathbf{Z}} - \mathbf{Z}^0\| \geq h)\right\} & \leq \frac{1}{nh^{r+1}} \sum_{i=1}^n E\|\hat{\mathbf{Z}} - \mathbf{Z}^0\| \leq \frac{1}{n} \sum_{i=1}^n h^{-r-1} \tau_n \rightarrow 0. \end{aligned}$$

This implies that  $\|\hat{\mu}_j - \tilde{\mu}_j\| = O_p(h^{j-1} \tau_n)$  for  $j = 0, 1, 2$ . It follows that

$$|\hat{\sigma}^2 - \tilde{\sigma}^2| = O_p(h^{-1} \tau_n) \quad \text{and} \quad \left\| \frac{\hat{\mu}_1^\top \hat{\mu}_2^{-1}}{\hat{\sigma}^2} - \frac{\tilde{\mu}_1^\top \tilde{\mu}_2^{-1}}{\tilde{\sigma}^2} \right\| = O_p(h^{-2} \tau_n).$$

Thus, due to  $E\{\rho_j(\mathbf{Z}_i^0, \mathbf{Z}^0)\} = O(h^j \mathbf{1}^{\oplus j})$  and  $E[\{\rho_j(\mathbf{Z}_i^0, \mathbf{Z}^0)\}^{\oplus 2}] = O(h^{2j-r} \mathbf{1}^{\oplus 2j})$  for  $j = 0, 1$ , we have

$$\frac{1}{n} \sum_{i=1}^n \{\hat{w}(\hat{\mathbf{Z}}_i, \hat{\mathbf{Z}}, h) - \tilde{w}(\mathbf{Z}_i^0, \mathbf{Z}^0, h)\} = O_p(h^{-1} \tau_n).$$

□

## S.8 Additional Simulations for Networks

We consider graph Laplacians of undirected weighted networks with a fixed number of nodes  $m$  and bounded edge weights as a second type of metric-space valued responses; see Example 2. The space of graph Laplacians (Zhou and Müller, 2022) is

$$\Omega = \{Y = (y_{ij}) : Y = Y^\top; Y \mathbf{1}_m = 0_m; -W \leq y_{ij} \leq 0 \text{ for } i \neq j\}, \quad (34)$$

where  $1_m$  and  $0_m$  are the  $m$ -vectors of ones and zeroes, respectively. We aim to construct a generative model that produces random graph Laplacians  $Y$  along with an Euclidean predictor  $\mathbf{X} \in \mathbb{R}^9$ .

Denote the half vectorization excluding the diagonal of a symmetric and centered matrix by  $\text{vech}$ , with inverse operation  $\text{vech}^{-1}$ . By the symmetry and centrality of graph Laplacians as per (34), every graph Laplacian  $Y$  is fully determined by its upper (or lower) triangular part, which can be further vectorized into  $\text{vech}(Y)$ , a vector of length  $d = m(m - 1)/2$ . The true regression function can thus be defined as

$$m(\mathbf{X}) = \text{vech}^{-1}[\{-E(l_1|\mathbf{X}), \dots, -E(l_d|\mathbf{X})\}^T].$$

To generate random response  $Y$ , each entry of the random vector  $(l_1, \dots, l_d)^T$  is first generated using beta distributions whose parameters depend on the predictor  $\mathbf{X}$ . The random response  $Y$  is then generated conditional on  $\mathbf{X}$  through an inverse half vectorization  $\text{vech}^{-1}$  applied to  $(-l_1, \dots, -l_d)^T$ . The space of graph Laplacians  $\Omega$  is not a vector space. Instead, it is a bounded, closed, and convex subset in  $\mathbb{R}^{m^2}$  of dimension  $m(m - 1)/2$ . To ensure that the random response  $Y$  generated in simulations resides in  $L_m$ , the off-diagonal entries  $l_j$ ,  $j = 1, \dots, d$ , need to be nonpositive and bounded below as per (34). To this end, we consider

$$Y = \text{vech}^{-1}(-l_1, \dots, -l_d), \text{ where } l_j \stackrel{\text{i.i.d.}}{\sim} \text{Beta}(\alpha_1, \alpha_2),$$

$$\alpha_1 = X_8 \sin(\pi X_1) + (1 - X_8) \cos(\pi X_2),$$

$$\alpha_2 = X_4^2 X_7 + X_5^2 (1 - X_7),$$

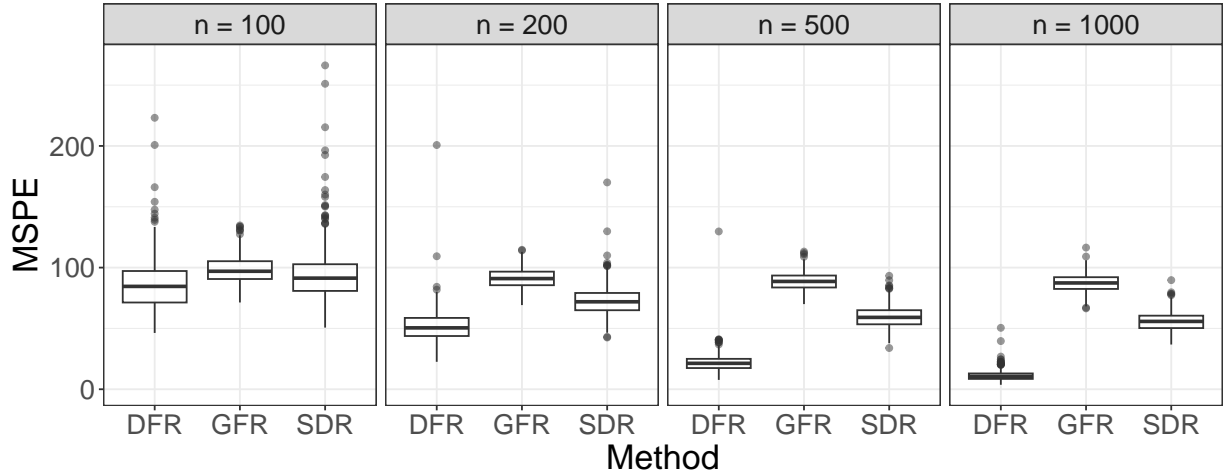


Figure 5: Boxplot of mean squared prediction errors for  $Q = 500$  Monte Carlo runs using deep Fréchet regression (the proposed method), global Fréchet regression (Zhou and Müller, 2022) and sufficient dimension reduction (Zhang et al., 2023) for network responses.

where components of the predictor  $\mathbf{X} \in \mathbb{R}^9$  are distributed as

$$X_1 \sim U(0, 1), \quad X_2 \sim U(-1/2, 1/2), \quad X_3 \sim U(1, 2)$$

$$X_4 \sim N(0, 1), \quad X_5 \sim N(0, 1), \quad X_6 \sim N(5, 5)$$

$$X_7 \sim \text{Ber}(0.4), \quad X_8 \sim \text{Ber}(0.3), \quad X_9 \sim \text{Ber}(0.6).$$

The true regression function is thus

$$m(\mathbf{X}) = \text{vech}^{-1}(-\alpha_1/(\alpha_1 + \alpha_2), \dots, -\alpha_1/(\alpha_1 + \alpha_2)).$$

Similar to simulations for the distributional data, we investigated sample sizes  $n = 100, 200, 500, 1000$ , with  $Q = 500$  Monte Carlo runs and set  $r = 2$  as the dimension of low-dimensional representations of random objects. We compare the proposed model with global Fréchet regression (GFR) and sufficient dimension reduction (SDR). Figure 5 displays the MSPE for various sample sizes across all Monte Carlo runs, while Table 3 summarizes their averages. We observe that MSPE decreases with increasing sample size, highlighting the convergence of the proposed methods. Both the boxplot and the table

Table 3: Average mean squared prediction error of deep Fréchet regression (the proposed method), global Fréchet regression (Petersen and Müller, 2019) and sufficient dimension reduction (Zhang et al., 2023) for network responses.

n	DFR	GFR	SDR
100	86.786	98.140	94.097
200	52.621	91.330	72.476
500	22.929	88.668	59.481
1000	11.189	87.518	55.782

illustrate the superior performance of the proposed model over GFR and SDR, even with small sample sizes. Despite the simulated network data not residing on a 2-dimensional manifold, the proposed model exhibits remarkable robustness as the sample size increases. Indeed, as the sample size grows, the proposed model proves to be a superior method for handling multivariate predictors and metric-space valued responses.

## S.9 Data Application for Human Mortality Data

We illustrate the proposed method using the age-at-death distributions of 162 countries in 2015, obtained from United Nations databases (<http://data.un.org/>) and UN World Population Prospects 2022 Databases (<https://population.un.org/wpp/Download>). For each country and age, the life table contains the number of deaths aggregated every five years, which can be treated as histograms of the number of deaths at age, with bin widths equal to 5 years. We use the `frechet` package (Chen et al., 2023) to create the density by local linear smoother on the histograms and finally standardize the function by trapezoid integration. Mortality distribution in each country is influenced by various factors, such as economics, healthcare systems, and social and environmental factors. To investigate these potential factors, we consider nine predictors, as used in Zhang et al. (2023), including demographic, economic, and environmental factors in 2015; see Table 4.



Table 4: Predictors of human mortality data.

Category	Variables	Explanation
Demography	1. population Density	Population per square Kilometer
	2. Sex Ratio	number of males per 100 females in the population
	3. Mean Childbearing Age	average age of mothers at the birth of their children
Economics	4. GDP	gross domestic product per capita
	5. GVA by Agriculture	percentage of agriculture, hunting, forestry, and fishing activities of gross value added
	6. CPI	consumer price index treating 2010 as the base year
	7. Unemployment Rate	percentage of unemployed people in the labor force
	8. Health Expenditure	percentage of expenditure on health of GDP
Environment	9. Arable Land	percentage of total land area

Table 5: Average mean squared prediction error of deep Fréchet regression (the proposed method), global Fréchet regression (Petersen and Müller, 2019) and sufficient dimension reduction (Zhang et al., 2023) for human mortality data.

DFR	GFR	SDR
26.2774	31.3276	27.0269

The MSPE was calculated through leave-one-out cross-validation. From Table 5, the proposed method achieves the most accurate prediction results, with a 16% and 3% improvement compared to GFR and SDR, respectively. These results demonstrate that despite the data not residing on a two-dimensional manifold and with a small sample size, the proposed method is superior and robust.

Additionally, our proposed method also allows for the investigation of the effects of predictors. Here, we further investigate the effect of GDP and health expenditure on mortality distributions while holding other predictors constant at their median values. Figure 6

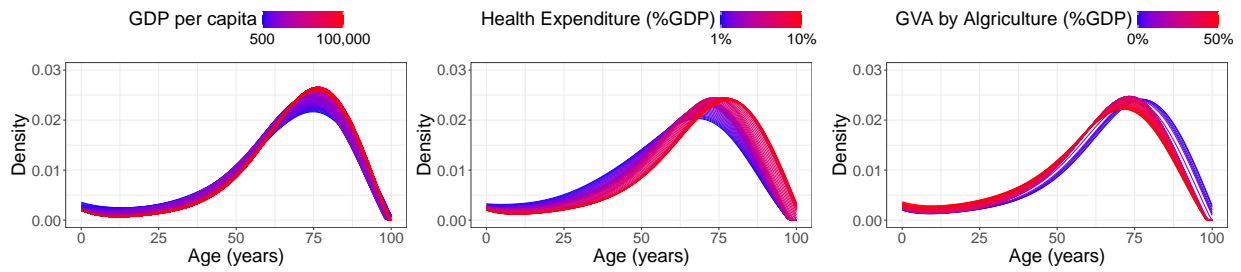


Figure 6: Age-at-death densities at different levels of GDP (left), health expenditure (middle) and agricultural GVA (right).

(left) shows that the fitted age-at-death densities shift towards the right as GDP increases, indicating an increase in life expectancy. Additionally, the probability of death before age 5 declines with increasing GDP, suggesting a lower infant mortality rate. Similarly, as the percentage of health expenditure in GDP increases, the age-at-death densities also shift rightward, indicating improved life expectancy. Conversely, as the percentage of agricultural GVA increases, the age-at-death densities shift leftward, indicating a decrease in life expectancy. This trend is consistent with the observation that as a country develops, GDP increases and the agricultural share of GVA commonly decreases.